A MUSCL-scheme on staggered unstructured grids for the Euler equations

Charbel Ghosn*, Thierry Goudon†, Sebastian Minjeaud‡

Université Côte d'Azur, CNRS, Inria, LJAD
Parc Valrose, F-06108 Nice, France

Abstract

We introduce MUSCL reconstructions for schemes designed on staggered grids for the numerical resolution of the Euler system. The proposed scheme uses principles based on the Discrete Duality Finite Volume framework for which the structure of the unknowns makes the gradient reconstruction naturally amenable. Dealing with general unstructured meshes, we develop a multislope approach where gradients and limiters are constructed face-by-face of the control volumes. Since the numerical unknowns are stored on different grids, several reconstruction techniques have to be combined. We study the stability conditions induced by the preservation of the positivity of the density and internal energy. The scheme is challenged against several numerical test cases.

Keywords: Euler equations. Staggered grids. MUSCL-scheme. Discrete Duality Finite Volume.

Contents

*cghosn@unice.fr
†thierry.goudon@inria.fr
‡sebastian.minjeaud@unice.fr

1 Introduction

This work is concerned with the simulation of the Euler system of gas dynamics

$$\begin{cases} \partial_t \rho + \boldsymbol{\nabla} \cdot \big(\rho \mathbf{u}\big) = 0, \\ \partial_t \big(\rho \mathbf{u}\big) + \boldsymbol{\nabla} \cdot \big(\rho \mathbf{u} \otimes \mathbf{u}\big) + \boldsymbol{\nabla} p = 0, \\ \partial_t \big(\rho E\big) + \boldsymbol{\nabla} \cdot \big(\rho E \mathbf{u}\big) + \boldsymbol{\nabla} \cdot \big(p \mathbf{u}\big) = 0. \end{cases} \tag{1}$$

The unknowns depend on the time and space variables $(t, x) \in [0, \infty) \times \Omega$ with $\Omega \subset \mathbb{R}^2$, a regular and bounded domain. In (1), ρ, $\mathbf{u}$, E and p stand for the mass density, the velocity field, the total energy and the pressure respectively. The pressure is related to the independent unknowns $(\rho, \mathbf{u}, E)$ through an equation of state; here we deal with the perfect gas law: given the adiabatic exponent $\gamma > 1$, we have

$$E = \frac{\|\mathbf{u}\|^2}{2} + e \text{ and } p = (\gamma - 1)\rho e,$$

where e is the internal energy.

Most of the numerical methods for the simulation of the Euler system (1) work with colocalized unknowns: in the finite volume framework, the numerical unknown represents the full vector of conserved quantities $(\rho, \rho u, \rho E)$ on the cells that realize the tessellation of Ω and the definition of the scheme relies on a suitable definition of the numerical fluxes on the interfaces of these cells; detailed presentations can be found in the classical treatises [8, 22, 24, 41, 49]. An alternative viewpoint uses staggered grids, storing densities/internal energies and velocities in different locations, see [52, 54]. This approach has been developed also for dealing with the Shallow-Water system [21, 32]. A strong motivation for developing the staggered framework comes from models or regimes involving constraints [6, 23, 33, 34, 35]. This is the case in low Mach regimes where prohibitive stability constraints or even a dramatic loss of accuracy have been identified with standard colocalized methods [17, 18, 30, 31].

This contribution is part of a series of works initialized in [5], where an original method on staggered grids has been introduced for the one-dimensional barotropic Euler equation. It is further developed to handle complex systems for mixture flows [6], and then adapted to deal with the multi-dimensional Euler system, when working on Cartesian grids [28], or on unstructured grids in [29]. When dealing with the full Euler system, a specific difficulty arises for schemes on staggered grids with the treatment of the energy equation. Since the total energy mixes up quantities stored on different grids, it is more convenient to work on the evolution equation for the internal energy. It is a well established fact, however, that the derivation from (1) holds assuming the regularity of the solutions, and, since discontinuities appear in finite time, correction terms should be incorporated. Suitable corrections in the design of numerical schemes based on the internal energy equations come from the discrete kinetic energy balance [23, 28, 29, 35]. Coming back to a discrete conservation law for the total energy is far from obvious. In order to address this issue, we have found advantages in developing an approach

based on the Discrete Duality Finite Volume (DDFV) framework. It has been introduced in the 2000s [20, 36], for solving the Laplace equation on general 2D meshes, including non-conformal ones. Since then, it has been successfully extended to general elliptic operators and for the simulation of viscous flows [9, 16, 26, 27, 39]. While initially developed for elliptic operators, these techniques can equally be fruitfully utilised for analysing the Euler system (1) discretized on staggered grids: identifying the duality relation between the discrete gradient and divergence operators, they allow us to make consistent transfer procedures appear between the different grids [29]; in turn, it leads to a discrete version of the *local* conservation of the total energy.

So far, the scheme introduced in [29] is only first-order accurate. This paper is concerned with the design of procedures to improve its accuracy. To this end, we shall make use of the MUSCL formalism. The MUSCL approach has been introduced by B. Van Leer [51] for one dimensional hyperbolic problems, see also [41, Chap. 16] or [49, Chapters 13 & 14]. The idea consists in using piecewise linear reconstruction in order to define more precise evaluation on the interfaces of the control volumes, that can be incorporated in the numerical fluxes. The polynomial interpolation has to be coupled to suitable slope/flux limitations in order to prevent spurious oscillations in presence of discontinuities of the solutions or near local extrema: in such situations the scheme is degraded by coming back to the first order numerical fluxes. The 1D method can be readily extended to multidimensional problems on Cartesian grids, just proceeding direction-wise [15]. However, quite surprisingly, the natural multidimensional extension fails in satisfying the TVD property [25], and one restricts to the requirement of a local maximum principle [53]. Dealing with unstructured meshes, which becomes necessary when the geometry of the computational domain becomes complex, leads to the question of the definition of the slope in the interpolation process, which cannot be deduced by a direct application of the mere 1D principle. Hence, the MUSCL technique can be adapted by defining a gradient on each cell, together with an appropriate limiter preventing the formation of spurious oscillations [2, 3, 4, 10, 19, 37, 38, 42]. A substantial gain of accuracy can be expected by introducing instead gradient and limiters on each of the interfaces of the control volumes. Indeed, the monoslope reconstruction is limited *globally*, accounting for the worst situation [10, 11, 13, 14, 40], while the multislope approach might relax the limitation in certain directions. In what follows, we adopt this mutislope approach for constructing a MUSCL-like scheme on unstructured staggered grids for (1). However, since we are working with different grids, we need to adopt different reconstructions, inspired by [11], [40] and [7], the latter being in the DDFV-fashion.

The paper is organized as follows. In Section 2, we set up the definitions of the meshes. Section 3 recaps the basis of the first-order scheme introduced in [29]. Section 4 details the reconstruction procedure: densities/internal energies and velocities being on different grids, with different geometrical properties, they are defined by using different interpolation methods. Note that all the geometrical quantities entering into the definition of the scheme can be computed once for all before computing the time evolution of the fluid (as far as the mesh is not modified by some refinement strategy). We pay a specific attention to the treatment of contact discontinuities. We discuss the constraint on the time step that garanties the positivity of the density. Finally, numerical simulations are presented in Section 5.

2 Notations, meshes, unknowns

From now on, we suppose that Ω is an open bounded polygonal domain of $\mathbb{R}^2$ and its boundary is denoted $\partial\Omega$. We construct three meshes covering Ω: the primal mesh, the dual mesh and the diamond mesh. The steps of the construction are illustrated in Fig. 1 and we adopt the same notations as in [29].

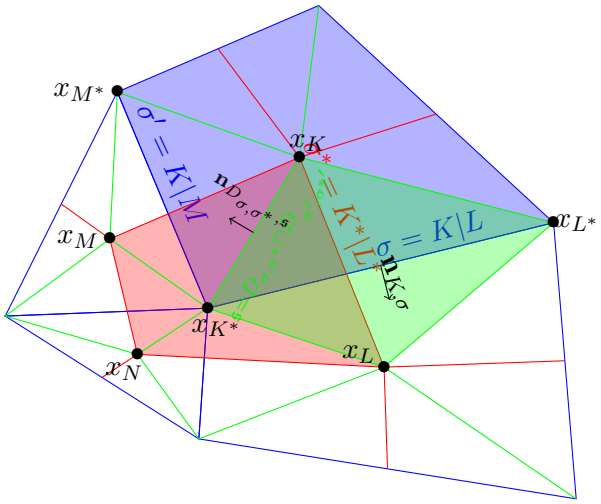

Figure 1: Meshes and associated notations.

1. The primal mesh $\mathfrak{M}$ is composed of disjoint, non-degenerate, convex polygons K called "primal cells". The centers of these cells are labeled x_K (as shown with the cells having blue edges in Fig. 1).
2. The dual mesh $\mathfrak{M}^* \cup \partial\mathfrak{M}^*$ consists of cells built "around the vertices x_{K^*}" of the primal mesh, see the cells with red edges in Fig. 1. More precisely, the interior dual mesh $\mathfrak{M}^*$ is made up of cells K^* formed by joining the centers x_K of all cells having K^* as a vertex. When $x_{K^*} \in \partial\Omega$, a dual cell is made by joining the centers of the cells that share the vertex x_{K^*} and the centers of the two boundary edges containing x_{K^*}.
3. The diamond mesh $\mathfrak{D}$ is composed of quadrilateral cells D_{σ,σ^*} obtained by joining the endpoints of the edges $\sigma = [x_{K^*}, x_{L^*}]$ of the primal mesh to the centers x_K and x_L of the primal mesh cells that share this edge — the latter defines an edge denoted $\sigma^* = [x_K, x_L]$ — see the cells with green edges in Fig. 1. We distinguish the diamonds of the boundary $\mathfrak{D}_{ext} = \{D_{\sigma,\sigma^*} \in \mathfrak{D} \text{ such that } \sigma \in \partial\Omega\}$ and $\mathfrak{D}_{int} = \mathfrak{D} \setminus \mathfrak{D}_{ext}$. In the specific case where $D_{\sigma,\sigma^*} \in \mathfrak{D}_{ext}$, the diamond cell D_{σ,σ^*} degenerates to a triangle.

Of course, the three meshes cover the computational domain:

$$\Omega = \bigcup_{K\in\mathfrak{M}} K = \bigcup_{K^*\in\mathfrak{M}^*\cup\partial\mathfrak{M}^*} K^* = \bigcup_{D_{\sigma,\sigma^*}\in\mathfrak{D}} D_{\sigma,\sigma^*}.$$

A mesh is thus defined as a pair $(\mathfrak{T}, \mathfrak{D})$ where $\mathfrak{T} = \mathfrak{M} \cup \mathfrak{M}^* \cup \partial\mathfrak{M}^*$ combines the primal mesh $\mathfrak{M}$ and the dual mesh $\mathfrak{M}^* \cup \partial\mathfrak{M}^*$ and $\mathfrak{D}$ stands for the associated diamond mesh. Note that contrarily to standard DDFV notation, we do not introduce here the notation $\partial\mathfrak{M}$ for the set of edges of the primal mesh $\mathfrak{M}$ included in $\partial\Omega$, considered as degenerate cells.
We also refer the reader to Fig. 1 for the following notations:

1. We denote $\mathfrak{s} = D_{\sigma,\sigma^*}|D_{\sigma',\sigma^{*\prime}}$ the face separating two diamond cells D_{σ,σ^*} and $D_{\sigma',\sigma^{*\prime}}$.
2. For $K \in \mathfrak{M}$, we denote $\mathfrak{D}_K = \{D_{\sigma,\sigma^*} \in \mathfrak{D}, \sigma \in \partial K\}$. For $K^* \in \mathfrak{M}^* \cup \partial\mathfrak{M}^*$, we similarly denote $\mathfrak{D}_{K^*} = \{D_{\sigma,\sigma^*} \in \mathfrak{D}, \sigma^* \in \partial K^*\}$.
3. For a cell X of $\mathfrak{M}$, $\mathfrak{M}^* \cup \partial\mathfrak{M}^*$ or $\mathfrak{D}$ and for $\mathfrak{x} \in \partial X$, we define a unit vector $\mathbf{n}_{X,\mathfrak{x}}$ normal to the face $\mathfrak{x}$ of the cell X and pointing outwards: $\mathbf{n}_{K,\sigma}$ (with $\sigma \in \partial K$ for $K \in \mathfrak{M}$), $\mathbf{n}_{K^*,\sigma^*}$

(with $\sigma^* \in \partial K^*$ for $K^* \in \mathfrak{M}^*$), and $\mathbf{n}_{D_{\sigma,\sigma^*},\mathfrak{s}}$ (with $\mathfrak{s} \in \partial D_{\sigma,\sigma^*}$ for $D_{\sigma,\sigma^*} \in \mathfrak{D}$). Note that, for $\sigma = K|L$, for $\sigma^* = K^*|L^*$ and for $\mathfrak{s} = D_{\sigma,\sigma^*}|D_{\sigma',\sigma^{*\prime}}$, we have

$$\mathbf{n}_{K,\sigma} = -\mathbf{n}_{L,\sigma}, \qquad \mathbf{n}_{K^*,\sigma^*} = -\mathbf{n}_{L^*,\sigma^*}, \qquad \mathbf{n}_{D_{\sigma,\sigma^*},\mathfrak{s}} = -\mathbf{n}_{D_{\sigma',\sigma^{*\prime}},\mathfrak{s}}.$$

The unknowns of the scheme are defined as piecewise constants over the cells :

1. Density, internal energy and pressure are piecewise constants over the diamond cells; alternatively, we can think of quantities stored on the edges of the initial mesh: ρ_{σ,σ^*} and e_{σ,σ^*} are constant on the diamond cell $D_{\sigma,\sigma^*} \in \mathfrak{D}$ and we set $p_{\sigma,\sigma^*} = (\gamma-1)\rho_{\sigma,\sigma^*}e_{\sigma,\sigma^*}$.
2. The numerical velocity fields are piecewise constants over the primal and dual cells, stored at both the centers and the vertices of the cell of the primal mesh: $\mathbf{u}_K$ is constant on the primal cell $K \in \mathfrak{M}$ and $\mathbf{u}_{K^*}$ is constant on the dual cell $K^* \in \mathfrak{M}^* \cup \partial\mathfrak{M}^*$.

Observe that, in contrast to the Cartesian framework [28], we store all the components of the velocity on the centers and vertices of the primal meshes.

Definition 2.1. For $\mathfrak{s} = D_{\sigma,\sigma^*}|D_{\sigma',\sigma^{*\prime}}$, we denote

$$e_{\mathfrak{s}} := \frac{e_{\sigma,\sigma^*} + e_{\sigma',\sigma^{*\prime}}}{2}.$$

For $\mathfrak{s} = [x_K, x_{K^*}]$ an edge of D_{σ,σ^*}, we denote

$$u_{D_{\sigma,\sigma^*},\mathfrak{s}} := \frac{\mathbf{u}_K + \mathbf{u}_{K^*}}{2} \cdot \mathbf{n}_{D_{\sigma,\sigma^*},\mathfrak{s}}.$$

It is worth observing that

$$u_{D_{\sigma,\sigma^*},\mathfrak{s}} = -u_{D_{\sigma',\sigma^{*\prime}},\mathfrak{s}} \quad \text{if} \quad \mathfrak{s} = D_{\sigma,\sigma^*}|D_{\sigma',\sigma^{*\prime}}.$$

3 First order scheme

We remind the reader the construction of the scheme proposed in [29] and its main properties.

3.1 Definition of the scheme: numerical fluxes, discrete gradient and divergence operators

We introduce the sound speed of (1): $c(e) = \sqrt{\gamma(\gamma-1)e}$ and the functions

$$(u,c) \in \mathbb{R} \times (0,\infty) \longmapsto \lambda_\pm(u,c) = u \pm c.$$

(In 1D, together with u, they are the characteristic speeds of the system (1); in multi-D, we need the characteristic speeds associated to a direction $\xi \in \mathbb{S}^1$, $\mathbf{u}\cdot\xi$ and $\lambda_\pm(\mathbf{u}\cdot\xi, c)$.) The definition of the numerical fluxes uses the functions $(\rho,u,c) \in (0,\infty)\times\mathbb{R}\times(0,\infty) \longmapsto \mathcal{F}^\pm(\rho,u,c)$ given by

$$\mathcal{F}^+(\rho,c,u) = \begin{cases} 0 & \text{if } u \leqslant -c, \\ \dfrac{\rho}{4c}\lambda_+(u,c)^2 & \text{if } |u| \leqslant c, \\ \rho u & \text{if } u \geqslant c, \end{cases} \tag{2}$$

and

$$\mathcal{F}^-(\rho,c,u) = \begin{cases} \rho u & \text{if } u \leqslant -c, \\ -\dfrac{\rho}{4c}\lambda_-(u,c)^2 & \text{if } |u| \leqslant c, \\ 0 & \text{if } u \geqslant c. \end{cases} \tag{3}$$

The scheme is based on a splitting of the mass flux inspired from the framework of kinetic schemes (see e. g. [46] for further details) applying upwinding principles to the first moment of the "Maxwellian"

$$\xi \in \mathbb{R} \longmapsto \mathcal{M}_{[\rho,c,u]}(\xi) = \frac{\rho}{2c}\mathbb{1}_{|\xi-u|\leqslant c},$$

leading to

$$\mathcal{F}^{\pm} = \int_{\xi \gtrless 0} \xi \mathcal{M} \, \mathrm{d}\xi.$$

Given an interface, the mass flux associated with positive (or negative) kinetic velocities ξ is determined using the backward (or frontward) density. This definition significantly diverges from the approach presented in [33, 34, 35], which relies exclusively on the material velocity u and does not consider characteristic speeds, aligning instead with the principles of AUSM schemes [44, 43]. Consequently, it inherently introduces some numerical diffusion, effectively preventing the occurrence of oscillations as the material velocity u becomes small, as discussed in [5, Appendix B]. The functions $\mathcal{F}^{\pm}$ satisfy the following properties, which are crucial for the analysis of the scheme:

- symmetry :
$$\mathcal{F}^{-}(\rho, c, u) = -\mathcal{F}^{+}(\rho, c, -u), \tag{4}$$
- consistency :
$$\mathcal{F}^{+}(\rho, c, u) + \mathcal{F}^{-}(\rho, c, u) = \rho u, \tag{5}$$
- for any $u \in \mathbb{R}$, $\rho \geqslant 0$ and $c \geqslant 0$, we have
$$0 \leqslant \mathcal{F}^{+}(\rho, c, u) \leqslant \rho[\lambda_{+}(c, u)]^{+} \quad \text{and} \quad -\rho[\lambda_{-}(c, u)]^{-} \leqslant \mathcal{F}^{-}(\rho, c, u) \leqslant 0. \tag{6}$$

We thus define the first order mass flux $\mathcal{F}_{D_{\sigma,\sigma^*},\mathfrak{s}}$ from the diamond cell D_{σ,σ^*} through the interface $\mathfrak{s} = D_{\sigma,\sigma^*}|D_{\sigma',\sigma^{*\prime}}$ using the upwind principle as follows

$$\mathcal{F}_{D_{\sigma,\sigma^*},\mathfrak{s}} = \mathcal{F}^{+}_{D_{\sigma,\sigma^*},\mathfrak{s}} + \mathcal{F}^{-}_{D_{\sigma,\sigma^*},\mathfrak{s}}$$

with

$$\mathcal{F}^{+}_{D_{\sigma,\sigma^*},\mathfrak{s}} = \mathcal{F}^{+}(\rho_{\sigma,\sigma^*}, c_{\mathfrak{s}}, u_{D_{\sigma,\sigma^*},\mathfrak{s}}) \quad \text{and} \quad \mathcal{F}^{-}_{D_{\sigma,\sigma^*},\mathfrak{s}} = \mathcal{F}^{-}(\rho_{\sigma',\sigma^{*\prime}}, c_{\mathfrak{s}}, u_{D_{\sigma,\sigma^*},\mathfrak{s}}), \tag{7}$$

where $c_{\mathfrak{s}} = c(e_{\mathfrak{s}})$, $e_{\mathfrak{s}}$ and the interface velocity $u_{D_{\sigma,\sigma^*},\mathfrak{s}}$ as in Definition 2.1.

The discrete mass equation on a cell $D_{\sigma,\sigma^*} \in \mathfrak{D}_{int}$ is given by

$$\frac{\overline{\rho}_{\sigma,\sigma^*} - \rho_{\sigma,\sigma^*}}{\delta t} + \frac{1}{|D_{\sigma,\sigma^*}|} \sum_{\mathfrak{s} \in \partial D_{\sigma,\sigma^*}} |\mathfrak{s}| \mathcal{F}_{D_{\sigma,\sigma^*},\mathfrak{s}} = 0. \tag{8}$$

Next, we introduce the averaged density on a cell K of the primal mesh, defined by

$$\rho_K = \sum_{D_{\sigma,\sigma^*} \in \mathfrak{D}_K} \frac{|D_{\sigma,\sigma^*} \cap K|}{|K|} \rho_{\sigma,\sigma^*} \text{ for } K \in \mathfrak{M}$$

and on a cell K^* of the dual mesh, we set

$$\rho_{K^*} = \sum_{D_{\sigma,\sigma^*} \in \mathfrak{D}_{K^*}} \frac{|D_{\sigma,\sigma^*} \cap K^*|}{|K^*|} \rho_{\sigma,\sigma^*} \text{ for } K^* \in \mathfrak{M}^* \cup \partial\mathfrak{M}^*.$$

To these densities we associate averaged mass fluxes $\mathcal{F}_{K,\sigma}$, outgoing from a primal cell K, and $\mathcal{F}_{K^*,\sigma^*}$, outgoing from a dual cell K^*, given by the formula

$$\mathcal{F}^{\pm}_{K,\sigma} = \frac{|D_{\sigma,\sigma^*} \cap K|}{|D_{\sigma,\sigma^*}|} \sum_{\substack{\mathfrak{s} \in \partial D_{\sigma,\sigma^*} \\ \mathfrak{s} \subset L}} \frac{|\mathfrak{s}|}{|\sigma|} \mathcal{F}^{\pm}_{D_{\sigma,\sigma^*},\mathfrak{s}} - \frac{|D_{\sigma,\sigma^*} \cap L|}{|D_{\sigma,\sigma^*}|} \sum_{\substack{\mathfrak{s} \in \partial D_{\sigma,\sigma^*} \\ \mathfrak{s} \subset K}} \frac{|\mathfrak{s}|}{|\sigma|} \mathcal{F}^{\mp}_{D_{\sigma,\sigma^*},\mathfrak{s}}. \tag{9}$$

$$\mathcal{F}^{\pm}_{K^*,\sigma^*} = \frac{|D_{\sigma,\sigma^*} \cap K^*|}{|D_{\sigma,\sigma^*}|} \sum_{\substack{\mathfrak{s} \in \partial D_{\sigma,\sigma^*} \\ \mathfrak{s} \subset L^*}} \frac{|\mathfrak{s}|}{|\sigma^*|} \mathcal{F}^{\pm}_{D_{\sigma,\sigma^*},\mathfrak{s}} - \frac{|D_{\sigma,\sigma^*} \cap L^*|}{|D_{\sigma,\sigma^*}|} \sum_{\substack{\mathfrak{s} \in \partial D_{\sigma,\sigma^*} \\ \mathfrak{s} \subset K^*}} \frac{|\mathfrak{s}|}{|\sigma^*|} \mathcal{F}^{\mp}_{D_{\sigma,\sigma^*},\mathfrak{s}}. \tag{10}$$

Remarkably, the averaged densities ρ_K, ρ_{K^*} satisfy the following conservative equations for any $K \in \mathfrak{M}$ and any $K^* \in \mathfrak{M}^* \cup \partial\mathfrak{M}^*$:

$$|K| \frac{\overline{\rho}_K - \rho_K}{\delta t} + \sum_{D_{\sigma,\sigma^*} \in \mathfrak{D}_K} |\sigma| \mathcal{F}_{K,\sigma} = 0, \tag{11}$$

$$|K^*| \frac{\overline{\rho}_{K^*} - \rho_{K^*}}{\delta t} + \sum_{D_{\sigma,\sigma^*} \in \mathfrak{D}_{K^*}} |\sigma^*| \mathcal{F}_{K^*,\sigma^*} + \sum_{D_{\sigma,\sigma^*} \in \mathfrak{D}_{K^*} \cap \mathfrak{D}_{ext}} \frac{|\sigma|}{2} \mathcal{F}_{\sigma} = 0. \tag{12}$$

The proof is fully detailed in [29]; it can be seen as a consistency property of the fluxes $\mathcal{F}_{K,\sigma}, \mathcal{F}_{K^*,\sigma^*}$.

Using the fluxes $\mathcal{F}^{\pm}_{K,\sigma}$, we can give the definition of the momentum fluxes $\mathcal{G}_{K,\sigma}$ for the primal cells and $\mathcal{G}_{K^*,\sigma^*}$ for the dual cells. They are still based on upwinding principles. We consider the case of interfaces $\sigma \not\subset \partial\Omega$. In this case, for the primal cells we set

$$\mathcal{G}_{K,\sigma} = \mathcal{F}^{+}_{K,\sigma} \mathbf{u}_K + \mathcal{F}^{-}_{K,\sigma} \mathbf{u}_L. \tag{13}$$

We define similarly the momentum fluxes $\mathcal{G}_{K^*,\sigma^*}$. The momentum equation also requires to introduce a discrete pressure gradient. It is obtained by mimicking the formula

$$\int_X \boldsymbol{\nabla} p = \int_{\partial X} p \mathbf{n}.$$

Definition 3.1. The discrete pressure gradient $\boldsymbol{\nabla_d} p$ is defined on $\mathfrak{T}$ by

$$(\boldsymbol{\nabla_d} p)_K = \frac{1}{|K|} \sum_{D_{\sigma,\sigma^*} \in \mathfrak{D}_K} |\sigma| p_{\sigma,\sigma^*} \mathbf{n}_{K,\sigma}, \qquad \text{for } K \in \mathfrak{M},$$

$$(\boldsymbol{\nabla_d} p)_{K^*} = \frac{1}{|K^*|} \sum_{D_{\sigma,\sigma^*} \in \mathfrak{D}_{K^*}} |\sigma| p_{\sigma,\sigma^*} \mathbf{n}_{K^*,\sigma^*}, \qquad \text{for } K^* \in \mathfrak{M}^*,$$

$$(\boldsymbol{\nabla_d} p)_{K^*} = \frac{1}{|K^*|} \sum_{D_{\sigma,\sigma^*} \in \mathfrak{D}_{K^*} \cap \mathfrak{D}_{int}} |\sigma^*| p_{\sigma,\sigma^*} \mathbf{n}_{K^*,\sigma^*} + \sum_{D_{\sigma,\sigma^*} \in \mathfrak{D}_{K^*} \cap \mathfrak{D}_{int}} \frac{|\sigma|}{2} p_{\sigma,\sigma^*} \mathbf{n}_{K,\sigma}, \quad \text{for } K^* \in \partial\mathfrak{M}^*.$$

For further purposes, we will need a discrete divergence operator, naturally inspired from

$$\int_X \boldsymbol{\nabla} \cdot \mathbf{u} = \int_{\partial X} \mathbf{u} \cdot \mathbf{n}.$$

Definition 3.2. The discrete divergence operator on a cell $D_{\sigma,\sigma^*} \in \mathfrak{D}$ is defined as

$$(\boldsymbol{\nabla_d} \cdot \mathbf{u})_{\sigma,\sigma^*} = \frac{1}{|D_{\sigma,\sigma^*}|} \sum_{\mathfrak{s} \in \partial D_{\sigma,\sigma^*}} |\mathfrak{s}| u_{D_{\sigma,\sigma^*},\mathfrak{s}},$$

when $D_{\sigma,\sigma^*} \in \mathfrak{D}_{int}$, while for $D_{\sigma,\sigma^*} \in \mathfrak{D}_{ext}$, we set

$$(\boldsymbol{\nabla_d} \cdot \mathbf{u})_{\sigma,\sigma^*} = \frac{1}{|D_{\sigma,\sigma^*}|} \sum_{\mathfrak{s} \in \partial D_{\sigma,\sigma^*} \setminus \partial\Omega} |\mathfrak{s}| u_{D_{\sigma,\sigma^*},\mathfrak{s}} + \frac{|\sigma|}{2|D_{\sigma,\sigma^*}|} \Big(\mathbf{u}_\sigma + \frac{\mathbf{u}_{K^*} + \mathbf{u}_{L^*}}{2} \Big) \cdot \mathbf{n}_{K,\sigma}.$$

Finally, the discrete momentum equation is given for $K \in \mathcal{M}$ and $K^* \in \mathcal{M}^*$ by

$$\begin{aligned}
&\frac{\overline{\rho}_K \overline{\mathbf{u}}_K - \rho_K \mathbf{u}_K}{\delta t} + \frac{1}{|K|} \sum_{D_{\sigma,\sigma^*} \in \mathfrak{D}_K} |\sigma| \mathcal{G}_{K,\sigma} + (\boldsymbol{\nabla_d} p)_K = 0, \\
&\frac{\overline{\rho}_{K^*} \overline{\mathbf{u}}_{K^*} - \rho_{K^*} \mathbf{u}_{K^*}}{\delta t} + \frac{1}{|K^*|} \sum_{D_{\sigma,\sigma^*} \in \mathfrak{D}_{K^*}} |\sigma^*| \mathcal{G}_{K^*,\sigma^*} \\
&\qquad + \frac{1}{|K^*|} \sum_{D_{\sigma,\sigma^*} \in \mathfrak{D}_{K^*} \cap \mathfrak{D}_{ext}} \frac{|\sigma|}{2} \mathcal{G}_{K^*,\sigma} \quad + (\boldsymbol{\nabla_d} p)_{K^*} = 0.
\end{aligned} \tag{14}$$

We turn to the equation for the internal energy. To this end, we need to define the correction term $\mathcal{R}_{\sigma,\sigma^*}$ that comes from the kinetic energy balance [33]. We start by introducing the kinetic energy fluxes $\mathcal{K}_{K,\sigma}$ from primal cells and $\mathcal{K}_{K^*,\sigma^*}$ from dual cells:

$$\mathcal{K}_{K,\sigma} = \mathcal{F}^+_{K,\sigma} \frac{\|\mathbf{u}_K\|^2}{2} + \mathcal{F}^-_{K,\sigma} \frac{\|\mathbf{u}_L\|^2}{2}, \quad \text{and} \quad \mathcal{K}_{K^*,\sigma^*} = \mathcal{F}^+_{K^*,\sigma^*} \frac{\|\mathbf{u}_{K^*}\|^2}{2} + \mathcal{F}^-_{K^*,\sigma^*} \frac{\|\mathbf{u}_{L^*}\|^2}{2}. \tag{15}$$

Multiplying the discrete momentum equation by $\mathbf{u}_K$ or $\mathbf{u}_{K^*}$, we get the following discrete balance of kinetic energy for $K \in \mathfrak{M}$ and $K^* \in \mathfrak{M}^* \cup \partial\mathfrak{M}^*$, respectively:

$$\frac{\overline{\rho}_K \frac{\|\overline{\mathbf{u}}_K\|^2}{2} - \rho_K \frac{\|\mathbf{u}_K\|^2}{2}}{\delta t} + \frac{1}{|K|} \sum_{D_{\sigma,\sigma^*} \in \mathfrak{D}_K} |\sigma| \mathcal{K}_{K,\sigma} + (\boldsymbol{\nabla_d} p)_K \cdot \overline{\mathbf{u}}_K = -\mathcal{R}_K, \tag{16}$$

$$\begin{aligned}
&\frac{\overline{\rho}_{K^*} \frac{\|\overline{\mathbf{u}}_{K^*}\|^2}{2} - \rho_{K^*} \frac{\|\mathbf{u}_{K^*}\|^2}{2}}{\delta t} + \frac{1}{|K^*|} \sum_{D_{\sigma,\sigma^*} \in \mathfrak{D}_{K^*}} |\sigma^*| \mathcal{K}_{K^*,\sigma^*} \\
&\qquad + \frac{1}{|K^*|} \sum_{D_{\sigma,\sigma^*} \in \mathfrak{D}_{K^*} \cap \mathfrak{D}_{ext}} \frac{|\sigma|}{2} \mathcal{K}_{K^*,\sigma} + (\boldsymbol{\nabla_d} p)_{K^*} \cdot \overline{\mathbf{u}}_{K^*} = -\mathcal{R}_{K^*},
\end{aligned} \tag{17}$$

where, according to [29], the remainder terms $\mathcal{R}_K$ and $\mathcal{R}_{K^*}$ are given by

$$\mathcal{R}_K = \frac{\overline{\rho}_K}{2\delta t} \|\overline{\mathbf{u}}_K - \mathbf{u}_K\|^2 + \frac{1}{|K|} \sum_{D_{\sigma,\sigma^*} \in \mathfrak{D}_K} |\sigma| \mathcal{F}^-_{K,\sigma} \left(\frac{\|\overline{\mathbf{u}}_K - \mathbf{u}_K\|^2}{2} - \frac{\|\overline{\mathbf{u}}_K - \mathbf{u}_L\|^2}{2} \right),$$

$$\begin{aligned}
\mathcal{R}_{K^*} = \frac{\overline{\rho}_{K^*}}{2\delta t} \|\overline{\mathbf{u}}_{K^*} - \mathbf{u}_{K^*}\|^2 &+ \frac{1}{|K^*|} \sum_{D_{\sigma,\sigma^*} \in \mathfrak{D}_{K^*}} |\sigma^*| \mathcal{F}^-_{K^*,\sigma^*} \left(\frac{\|\overline{\mathbf{u}}_{K^*} - \mathbf{u}_{K^*}\|^2}{2} - \frac{\|\overline{\mathbf{u}}_{K^*} - \mathbf{u}_{L^*}\|^2}{2} \right) \\
&+ \frac{1}{|K^*|} \sum_{D_{\sigma,\sigma^*} \in \mathfrak{D}_{K^*} \cap \mathfrak{D}_{ext}} \frac{|\sigma|}{2} \mathcal{F}^-_{\sigma} \left(\frac{\|\overline{\mathbf{u}}_{K^*} - \mathbf{u}_{K^*}\|^2}{2} - \frac{\|\overline{\mathbf{u}}_{K^*} - \mathbf{u}_{\sigma}\|^2}{2} \right).
\end{aligned}$$

The numerical fluxes for the internal energy (intended to approximate $\rho u \times e$) are defined as follows: for all $D_{\sigma,\sigma^*} \in \mathfrak{D}_{int}$ and $\mathfrak{s} = D_{\sigma,\sigma^*} | D_{\sigma',\sigma^{*\prime}} \in \partial D_{\sigma,\sigma^*}$, we set

$$\mathcal{E}_{D_{\sigma,\sigma^*},\mathfrak{s}} = e_{\sigma,\sigma^*} \mathcal{F}^+_{D_{\sigma,\sigma^*},\mathfrak{s}} + e_{\sigma',\sigma^{*\prime}} \mathcal{F}^-_{D_{\sigma,\sigma^*},\mathfrak{s}}. \tag{18}$$

The discrete internal energy equation is given by

$$\begin{aligned}\frac{\overline{\rho}_{\sigma,\sigma^*}\overline{e}_{\sigma,\sigma^*}-\rho_{\sigma,\sigma^*}e_{\sigma,\sigma^*}}{\delta t}+\frac{1}{|D_{\sigma,\sigma^*}|}\sum_{\mathfrak{s}\in\partial D_{\sigma,\sigma^*}}|\mathfrak{s}|\mathcal{E}_{D_{\sigma,\sigma^*},\mathfrak{s}}\\ +p_{\sigma,\sigma^*}\left(\boldsymbol{\nabla_d}\cdot\overline{\mathbf{u}}\right)_{\sigma,\sigma^*}=\mathcal{R}_{\sigma,\sigma^*},\quad\forall D_{\sigma,\sigma^*}\in\mathfrak{D}_{int}\end{aligned}\tag{19}$$

where

$$\mathcal{R}_{\sigma,\sigma^*}=\frac{|D_{\sigma,\sigma^*}\cap K|\mathcal{R}_K+|D_{\sigma,\sigma^*}\cap L|\mathcal{R}_L+|D_{\sigma,\sigma^*}\cap K^*|\mathcal{R}_{K^*}+|D_{\sigma,\sigma^*}\cap L^*|\mathcal{R}_{L^*}}{2|D_{\sigma,\sigma^*}|}.\tag{20}$$

This correction term balances the kinetic energy contributions that appear when summing the internal energy equation and the kinetic energy equations. This formulation leads to the derivation of the local conservation of the total energy.

3.2 Properties of the scheme

The first order scheme is proved to be positivity preserving scheme for the density and the internal energy under some CFL-like conditions. We the reader to [29] for detailed proof of these statements.

Proposition 3.3. *Let $\rho_{\sigma,\sigma^*}\geqslant 0$. We assume that the following CFL-like conditions are satisfied*

$$\begin{aligned}&\frac{\delta t}{|D_{\sigma,\sigma^*}|}\sum_{\mathfrak{s}\in\partial D_{\sigma,\sigma^*}}|\mathfrak{s}|[\lambda_+(c(e_\mathfrak{s}),u_{D_{\sigma,\sigma^*},\mathfrak{s}})]^+\leqslant 1, &&\forall D_{\sigma,\sigma^*}\in\mathfrak{D}_{int}\\ &\frac{\delta t}{|D_{\sigma,\sigma^*}|}\left[\sum_{\mathfrak{s}\in\partial D_{\sigma,\sigma^*}\backslash\partial\Omega}|\mathfrak{s}|[\lambda_+(c(e_\mathfrak{s}),u_{D_{\sigma,\sigma^*},\mathfrak{s}})]^+ +|\sigma|[\lambda_+(c(e_\sigma),u_\sigma)]^+\right]\leqslant 1, &&\forall D_{\sigma,\sigma^*}\in\mathfrak{D}_{ext}.\end{aligned}\tag{21}$$

Then, the non negativity of the density ρ_{σ,σ^*} is preserved: $\overline{\rho}_{\sigma,\sigma^*}\geqslant 0$.

A strenthened CFL condition is required to preserve the non negativity of the internal energy e_{σ,σ^*}. The main step of the proof consists in checking that the remainder terms $\mathcal{R}_K$ and $\mathcal{R}_{K^*}$ are non-negative. The analysis makes the following quantity appear

$$\begin{aligned}\mathrm{reg}\,(\mathfrak{T})=\sup\Bigg(&\left\{\frac{1}{\sin(\alpha_{D_{\sigma,\sigma^*}})},D_{\sigma,\sigma^*}\in\mathfrak{D}\right\}\cup\left\{\frac{h_{D_{\sigma,\sigma^*}}}{\sqrt{|D_{\sigma,\sigma^*}|}},\ D_{\sigma,\sigma^*}\in\mathfrak{D}\right\}\\ &\cup\left\{\frac{|D_{\sigma,\sigma^*}|}{|D_{\sigma,\sigma^*}\cap X|},\ X\in\mathfrak{T},D_{\sigma,\sigma^*}\in\mathfrak{D}_X\right\}\cup\left\{\frac{|X|}{|D_{\sigma,\sigma^*}|},\ X\in\mathfrak{T},D_{\sigma,\sigma^*}\in\mathfrak{D}_X\right\}\Bigg),\end{aligned}$$

where $0<\alpha_{D_{\sigma,\sigma^*}}\leq\pi/2$ is the angle between the two diagonals of the diamond cell D_{σ,σ^*}. It measures the regularity of the mesh: the higher $\mathrm{reg}\,(\mathfrak{T})$, the flatter the cells. It can be shown that $\mathrm{reg}\,(\mathfrak{T})\geq 2$.

Proposition 3.4. *Let $e_{\sigma,\sigma^*}\geqslant 0$ and $\rho_{\sigma,\sigma^*}\geqslant 0$, $\forall D_{\sigma,\sigma^*}\in\mathfrak{D}$. Let assume that the following CFL-like conditions are satisfied*

$$\begin{aligned}\frac{\delta t}{|D_{\sigma,\sigma^*}|}\Bigg(\mathrm{reg}\,(\mathfrak{T})^2\,\frac{|\sigma^*|+|\sigma|}{\sqrt{2}}c(e_{\sigma,\sigma^*})+\sum_{\mathfrak{s}\in\partial D_{\sigma,\sigma^*}}|\mathfrak{s}|\Big([u_{D_{\sigma,\sigma^*},\mathfrak{s}}]^+ +c(e_\mathfrak{s})\Big)\Bigg)\\ \leqslant\min\left(\frac{1}{\gamma},\frac{1}{1+\mathrm{reg}\,(\mathfrak{T})}\right),\qquad\forall D_{\sigma,\sigma^*}\in\mathfrak{D}_{int}\end{aligned}\tag{22}$$

$$\frac{\delta t}{|D_{\sigma,\sigma^*}|}\left(\mathrm{reg}\,(\mathfrak{T})^2\,\frac{|\sigma^*|+|\sigma|}{\sqrt{2}}c(e_{\sigma,\sigma^*})+\sum_{\mathfrak{s}\in\partial D_{\sigma,\sigma^*}\setminus\partial\Omega}|\mathfrak{s}|\Big([u_{D_{\sigma,\sigma^*},\mathfrak{s}}]^+ + c(e_{\mathfrak{s}})\Big)\right.$$
$$\left.+\,|\sigma|[\lambda_+(c(e_\sigma),u_\sigma)]^+ + |\sigma|\Lambda^-_{\sigma,\mathrm{Dir}}\right)\leqslant \min\left(\frac{1}{\gamma},\frac{1}{1+\mathrm{reg}\,(\mathfrak{T})}\right),\quad \forall D_{\sigma,\sigma^*}\in\mathfrak{D}_{ext} \tag{23}$$

with $\Lambda^-_{\sigma,\mathrm{Dir}}=\frac{1}{2}\frac{\rho_{\mathrm{Dir}}}{\rho_{\sigma,\sigma^*}}[\lambda_-(c(e_{\mathrm{Dir}}),u_{\mathrm{Dir}})]^-$ *if* σ *is a Dirichlet boudary and* 0 *otherwise. Then, the non negativity of the internal energy is preserved: we have* $\overline{e}_{\sigma,\sigma^*}\geqslant 0$, $\forall D_{\sigma,\sigma^*}\in\mathfrak{D}$.

We turn now to the conservation of the total energy. As shown in [29], a *local* conservation equation is written for the total energy $\rho_{\sigma,\sigma^*}E_{\sigma,\sigma^*}$, where the total energy E_{σ,σ^*} in the cell $D_{\sigma,\sigma^*}\in\mathfrak{D}_{int}$ is defined by $E_{\sigma,\sigma^*}=e_{\sigma,\sigma^*}+E^{\mathrm{kin}}_{\sigma,\sigma^*}$ with

$$E^{\mathrm{kin}}_{\sigma,\sigma^*}=\frac{|D_{\sigma,\sigma^*}\cap K|\frac{\rho_K\|\mathbf{u}_K\|^2}{2}+|D_{\sigma,\sigma^*}\cap L|\frac{\rho_L\|\mathbf{u}_L\|^2}{2}+|D_{\sigma,\sigma^*}\cap K^*|\frac{\rho_{K^*}\|\mathbf{u}_{K^*}\|^2}{2}+|D_{\sigma,\sigma^*}\cap L^*|\frac{\rho_{L^*}\|\mathbf{u}_{L^*}\|^2}{2}}{2|D_{\sigma,\sigma^*}|\rho_{\sigma,\sigma^*}}.$$

Proposition 3.5. *The discrete total energy* $\rho_{\sigma,\sigma^*}E_{\sigma,\sigma^*}$ *satisfies the following conservative equation on* $\mathfrak{D}_{int}$*:*

$$\frac{\overline{\rho}_{\sigma,\sigma^*}\overline{E}_{\sigma,\sigma^*}-\rho_{\sigma,\sigma^*}E_{\sigma,\sigma^*}}{\delta t}+\frac{1}{|D_{\sigma,\sigma^*}|}\sum_{\mathfrak{s}\in\partial D_{\sigma,\sigma^*}}|\mathfrak{s}|\mathcal{T}_{D_{\sigma,\sigma^*},\mathfrak{s}}+\frac{1}{|D_{\sigma,\sigma^*}|}\sum_{\mathfrak{s}\in\partial D_{\sigma,\sigma^*}}|\mathfrak{s}|q_{D_{\sigma,\sigma^*},\mathfrak{s}}=0,$$

where

- $\mathcal{T}_{D_{\sigma,\sigma^*},\mathfrak{s}}$ *is a conservative total energy flux through the interface* $\mathfrak{s}$ *of the diamond cell* D_{σ,σ^*}*,*
- $\frac{1}{|D_{\sigma,\sigma^*}|}\sum_{\mathfrak{s}\in\partial D_{\sigma,\sigma^*}}|\mathfrak{s}|q_{D_{\sigma,\sigma^*},\mathfrak{s}}$ *is a conservative discrete version of* $\boldsymbol{\nabla}\cdot(p\overline{\mathbf{u}})$ *on the diamond cell* D_{σ,σ^*}*.*

4 The muscl reconstruction on staggered grids

We discuss how we adapt the MUSCL principles to the staggered framework on unstructured grids. There are two ingredients: firstly, the construction of (formally) second order accurate quantities on the edges of the cells (primal, dual or diamond), the construction of which has to be adapted to the different type of cells; secondly, the definition of numerical fluxes and correction terms.

- For the mass flux, we keep unchanged the velocity which is already defined at the interface $\mathfrak{s}$; we only have to replace the upwind value ρ_{σ,σ^*} by a MUSCL reconstruction $\rho^{ML}_{D_{\sigma,\sigma^*},\mathfrak{s}}$ of the density. We shall also use a reconstruction of the internal energy $e^{ML}_{D_{\sigma,\sigma^*},\mathfrak{s}}$ which enters in the definition of the numerical fluxes (see below). This defines the upgraded mass flux $\mathcal{F}^{ML}_{D_{\sigma,\sigma^*},\mathfrak{s}}$.
- For the momentum flux, we define the convection flux $\mathcal{G}^{ML}_{K,\sigma}$ by averaging the upgraded mass fluxes $\mathcal{F}^{ML,\pm}_{K,\sigma}$, combined to a MUSCL reconstructed velocity $\mathbf{u}^{ML}_{K,\sigma}$ at the interfaces σ.
- For the internal energy fluxes, we combine the upgraded mass fluxes $\mathcal{F}^{ML}_{K,\sigma}$ with a MUSCL reconstructed internal energy $e^{ML}_{K,\sigma}$. However, a direct reconstruction of the internal energy by linear interpolation would produce a bad behaviour of the scheme for contact discontinuities, where the pressure should be kept constant across discontinuities. For this reason, we define a reconstruction $(\rho e)^{ML}_{D_{\sigma,\sigma^*},\mathfrak{s}}$ of the product ρe at the interface $\mathfrak{s}$ and then we

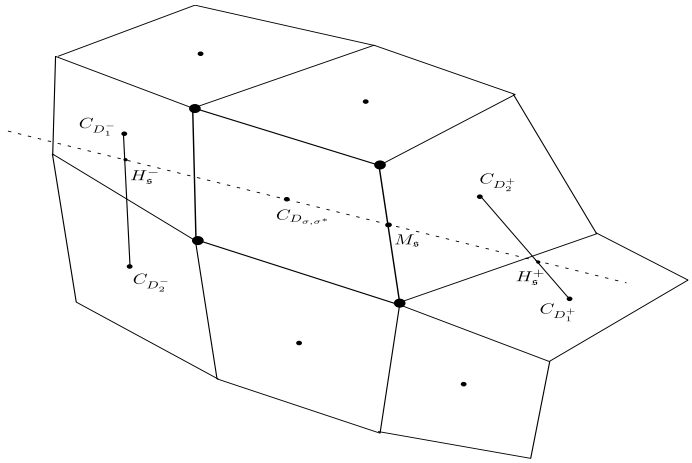

Figure 2: Forward and backward points $\mathbf{H}_{\mathfrak{s}}^+$ and $\mathbf{H}_{\mathfrak{s}}^-$

recover the internal energy through the ratio $\frac{(\rho e)^{ML}_{D_{\sigma,\sigma^*},\mathfrak{s}}}{\rho^{ML}_{D_{\sigma,\sigma^*},\mathfrak{s}}}$, see [48] for further comments on this issue. For the internal energy equation, we should also redefine the remainder terms $\mathcal{R}_K^{ML}, \mathcal{R}_{K^*}^{ML}$ and $\mathcal{R}_{\sigma,\sigma^*}^{ML}$ in terms of the new reconstructed variables and fluxes.

Let us now explain the reconstruction of the numerical unknowns, and how the geometry of the grids is taken into account.

4.1 Density and internal energy reconstruction, mass fluxes

For the density and the internal energy, we follow the multislope method introduced in [40]. As explained in the introduction, defining different slopes on each interface leads to a more accurate scheme than the monoslope method since it is subjected to less limitations. As in the original MUSCL method, both a backward and a forward scalar slope, denoted $s^-_{\sigma,\mathfrak{s}}$ and $s^+_{\sigma,\mathfrak{s}}$ respectively, are computed for each interface $\mathfrak{s}$ of a given diamond cell D_{σ,σ^*}. Unphysical oscillations are ruled out by means of a limiter function $\phi(s^-_{\sigma,\mathfrak{s}}, s^+_{\sigma,\mathfrak{s}})$, see [47]. Therefore, the reconstructed values, which are computed at the centers of the interfaces $\mathbf{M}_{\mathfrak{s}}$, read as follows:

$$\rho^{ML}_{D_{\sigma,\sigma^*},\mathfrak{s}} = \rho_{\sigma,\sigma^*} + \phi(s^-_{\sigma,\mathfrak{s}}, s^+_{\sigma,\mathfrak{s}}) \cdot ||\mathbf{C}_{D_{\sigma,\sigma^*}}\mathbf{M}_{\mathfrak{s}}||, \tag{24}$$

where $\mathbf{C}_{D_{\sigma,\sigma^*}}$ is the center of the diamond cell D_{σ,σ^*}, the intersection between the edges σ, σ^*.

The cornerstone of the scheme thus lies in the definition of the slopes. Let us denote by $\mathcal{W}_{\sigma,\sigma^*}$ the set of the diamond cells sharing at least a vertex with D_{σ,σ^*}. We need two points $\mathbf{H}_{\mathfrak{s}}^+$ and $\mathbf{H}_{\mathfrak{s}}^-$ both located on the axis $(\mathbf{C}_{D_{\sigma,\sigma^*}}\mathbf{M}_{\mathfrak{s}})$, respectively backward and forward the point $\mathbf{C}_{D_{\sigma,\sigma^*}}$ (see Fig. 2). A priori, these points are neither vertices of the grid, nor centers. Nevertheless, they can be used in a way to obtain second-order values of the variables, using a well chosen set of neighboring elements. Having computed the associated densities $\rho_{\mathbf{H}_{\mathfrak{s}}^-}$ and $\rho_{\mathbf{H}_{\mathfrak{s}}^+}$ at points $\mathbf{H}_{\mathfrak{s}}^+$ and $\mathbf{H}_{\mathfrak{s}}^-$, we obtain the backward and forward slopes as follows:

$$s^-_{\sigma,\mathfrak{s}} = \frac{\rho_{\sigma,\sigma^*} - \rho_{\mathbf{H}_{\mathfrak{s}}^-}}{||\mathbf{C}_{D_{\sigma,\sigma^*}}\mathbf{H}_{\mathfrak{s}}^-||}, \qquad s^+_{\sigma,\mathfrak{s}} = \frac{\rho_{\mathbf{H}_{\mathfrak{s}}^+} - \rho_{\sigma,\sigma^*}}{||\mathbf{C}_{D_{\sigma,\sigma^*}}\mathbf{H}_{\mathfrak{s}}^+||}.$$

We are left with the task of determining the points $\mathbf{H}_{\mathfrak{s}}^+$ and $\mathbf{H}_{\mathfrak{s}}^-$ in a 2D domain. To this end, we use the procedure described in [40]. Let $D_1^- \in \mathcal{W}_{\sigma,\sigma^*}$ be the most backward neighboring

diamond cell of D_{σ,σ^*} with respect to the direction $(\mathbf{C}_{D_{\sigma,\sigma^*}}\mathbf{M}_{\mathfrak{s}})$ and $\mathbf{C}_{D_1^-}$ its center. They are determined by

$$\cos\left(\mathbf{C}_{D_1^-}\mathbf{C}_{D_{\sigma,\sigma^*}},\mathbf{C}_{D_{\sigma,\sigma^*}}\mathbf{M}_{\mathfrak{s}}\right)=\max_{D\in\mathcal{W}_{\sigma,\sigma^*}}\cos\left(\mathbf{C}_D\mathbf{C}_{D_{\sigma,\sigma^*}},\mathbf{C}_{D_{\sigma,\sigma^*}}\mathbf{M}_{\mathfrak{s}}\right). \tag{25}$$

Now, let $\mathbf{C}_{D_2^-}$ be the center of the most backward diamond cell, located on the other side of the axis $(\mathbf{C}_{D_{\sigma,\sigma^*}}\mathbf{M}_{\mathfrak{s}})$; namely, we have

$$\cos\left(\mathbf{C}_{D_2^-}\mathbf{C}_{D_{\sigma,\sigma^*}},\mathbf{C}_{D_{\sigma,\sigma^*}}\mathbf{M}_{\mathfrak{s}}\right)=\max_{D\in\overline{\mathcal{W}}_{\sigma,\sigma^*}}\cos\left(\mathbf{C}_D\mathbf{C}_{D_{\sigma,\sigma^*}},\mathbf{C}_{D_{\sigma,\sigma^*}}\mathbf{M}_{\mathfrak{s}}\right), \tag{26}$$

with

$$\overline{\mathcal{W}}_{\sigma,\sigma^*}=\left\{D|D\in\mathcal{W}_{\sigma,\sigma^*},D\neq D_1^-,\sin\left(\mathbf{C}_D\mathbf{C}_{D_{\sigma,\sigma^*}},\mathbf{C}_{D_{\sigma,\sigma^*}}\mathbf{M}_{\mathfrak{s}}\right)\cdot\sin\left(\mathbf{C}_{D_1^-}\mathbf{C}_{D_{\sigma,\sigma^*}},\mathbf{C}_{D_{\sigma,\sigma^*}}\mathbf{M}_{\mathfrak{s}}\right)\leq 0\right\}.$$

Based on this construction, we define the point $\mathbf{H}_{\mathfrak{s}}^-$ as to be the intersection between the axis $(\mathbf{C}_{D_{\sigma,\sigma^*}}\mathbf{M}_{\mathfrak{s}})$ and the line $(\mathbf{C}_{D_1^-}\mathbf{C}_{D_2^-})$. The point $\mathbf{H}_{\mathfrak{s}}^-$lies in the segment $(\mathbf{C}_{D_1^-}\mathbf{C}_{D_2^-})$. Therefore, we introduce the barycentric coordinates of $\mathbf{H}_{\mathfrak{s}}^-$ with respect of $(\mathbf{C}_{D_1^-}\mathbf{C}_{D_2^-})$:

$$\alpha_1^-=\frac{||\mathbf{C}_{D_2^-}\mathbf{H}_{\mathfrak{s}}^-||}{||\mathbf{C}_{D_1^-}\mathbf{C}_{D_2^-}||}\geq 0,\qquad \alpha_2^-=\frac{||\mathbf{C}_{D_1^-}\mathbf{H}_{\mathfrak{s}}^-||}{||\mathbf{C}_{D_1^-}\mathbf{C}_{D_2^-}||}\geq 0,\qquad \alpha_1^-+\alpha_2^-=1.$$

In a symmetric way, we determine the points $\mathbf{C}_{D_1^+}$ and $\mathbf{C}_{D_2^+}$ for the forward direction (we consider the minimum instead of the maximum in (25) and (26)). Then $\mathbf{H}_{\mathfrak{s}}^+$ will be the intersection between $(\mathbf{C}_{D_{\sigma,\sigma^*}}\mathbf{M}_{\mathfrak{s}})$ and $(\mathbf{C}_{D_1^+}\mathbf{C}_{D_2^+})$, and we consider the barycentric coordinates

$$\alpha_1^+=\frac{||\mathbf{C}_{D_2^+}\mathbf{H}_{\mathfrak{s}}^+||}{||\mathbf{C}_{D_1^+}\mathbf{C}_{D_2^+}||}\geq 0,\quad \alpha_2^+=\frac{||\mathbf{C}_{D_1^+}\mathbf{H}_{\mathfrak{s}}^+||}{||\mathbf{C}_{D_1^+}\mathbf{C}_{D_2^+}||}\geq 0,\quad \alpha_1^++\alpha_2^+=1.$$

We point out that the computation of the coefficients $\alpha_1^\pm$ and $\alpha_2^\pm$ depends only on the mesh and it is performed once for all as a preliminary step of the code. Finally, we compute the densities at points $\mathbf{H}_{\mathfrak{s}}^-$ and $\mathbf{H}_{\mathfrak{s}}^+$ according to simple weighted means:

$$\rho_{\mathbf{H}_{\mathfrak{s}}^-}=\alpha_1^-\rho_{D_1^-}+\alpha_2^-\rho_{D_2^-},\quad \rho_{\mathbf{H}_{\mathfrak{s}}^+}=\alpha_1^+\rho_{D_1^+}+\alpha_2^+\rho_{D_2^+}.$$

Being a convex combination, the reconstructed values satisfy the same estimates as the $\rho_{D_j^\pm}$'s. We proceed similarly to reconstruct the values of the density of internal energy ρe which will be denoted by $(\rho e)^{ML}_{D_{\sigma,\sigma^*},\mathfrak{s}}$. The reconstructed internal energy by $e^{ML}_{D_{\sigma,\sigma^*},\mathfrak{s}}$ will be then the ratio $\frac{(\rho e)^{ML}_{D_{\sigma,\sigma^*},\mathfrak{s}}}{\rho^{ML}_{D_{\sigma,\sigma^*},\mathfrak{s}}}$. The upgraded mass flux will be

$$\mathcal{F}^{ML}_{D_{\sigma,\sigma^*},\mathfrak{s}}=\mathcal{F}^{ML,+}_{D_{\sigma,\sigma^*},\mathfrak{s}}+\mathcal{F}^{ML,-}_{D_{\sigma,\sigma^*},\mathfrak{s}}$$

with

$$F^{ML,+}_{D_{\sigma,\sigma^*},\mathfrak{s}}=\mathcal{F}^+(\rho^{ML}_{D_{\sigma,\sigma^*},\mathfrak{s}},c(e^{ML}_{D_{\sigma,\sigma^*},\mathfrak{s}}),u_{D_{\sigma,\sigma^*},\mathfrak{s}})\qquad \mathcal{F}^{ML,-}_{D_{\sigma,\sigma^*},\mathfrak{s}}=\mathcal{F}^-(\rho^{ML}_{D_{\sigma',\sigma^{*\prime}},\mathfrak{s}},c(e^{ML}_{D_{\sigma,\sigma^*},\mathfrak{s}}),u_{D_{\sigma,\sigma^*},\mathfrak{s}}). \tag{27}$$

For the diamond cell $D_{\sigma,\sigma^*}\in\mathfrak{D}_{ext}$, the outgoing mass flux $\mathcal{F}^{ML}_\sigma=\mathcal{F}^{ML,+}_\sigma+\mathcal{F}^{ML,-}_\sigma$ is defined as follows :

- $\mathcal{F}^{ML,+}_\sigma=0$ and $\mathcal{F}^{ML,-}_\sigma=0$ for zero-flux conditions,
- $\mathcal{F}^{ML,+}_\sigma=\mathcal{F}^+\left(\rho^{ML}_{\sigma,\sigma^*},c(e_\sigma),u_\sigma\right)$ and $\mathcal{F}^{ML,-}_\sigma=0$ for outflow conditions,
- $\mathcal{F}^{ML,+}_\sigma=\mathcal{F}^+(\rho^{ML}_{\sigma,\sigma^*},c(e_\sigma),u_\sigma)$ and $\mathcal{F}^{ML,-}_\sigma=\mathcal{F}^-(\rho_{\mathrm{Dir}},c(e_\sigma),u_\sigma)$ for Dirichlet conditions.

The internal energy flux is given by

$$\mathcal{E}^{ML}_{D_{\sigma,\sigma^*},\mathfrak{s}}=e^{ML}_{D_{\sigma,\sigma^*},\mathfrak{s}}\mathcal{F}^{ML,+}_{D_{\sigma,\sigma^*},\mathfrak{s}}+e^{ML}_{D_{\sigma',\sigma^{*\prime}},\mathfrak{s}}\mathcal{F}^{ML,-}_{D_{\sigma,\sigma^*},\mathfrak{s}}. \tag{28}$$

Contact discontinuity problem. We check the ability of the scheme in handling accurately contact discontinuities. We display the comparison between the first order method and the scheme obtained with the MUSCL reconstruction of the mass density and the density of internal energy. This can be compared to the method introduced in [23] which does not include a MUSCL reconstruction on the velocity, The computational domain is the slab $[0, 1]$ discretized with 256 equidistant grid points. We take $\gamma = 1.4$. The initial data ρ, u and p are piecewise constant functions with a discontinuity located at $x_0 = 0.5$.

	ρ_l	ρ_r	u_l	u_r	p_l	p_r	T
Test 1	1	0.125	0	0	1	0.1	0.25
Test 2	1	1	0	0	1000	0.1	0.012

Table 1: Data for 1D contact discontinuities

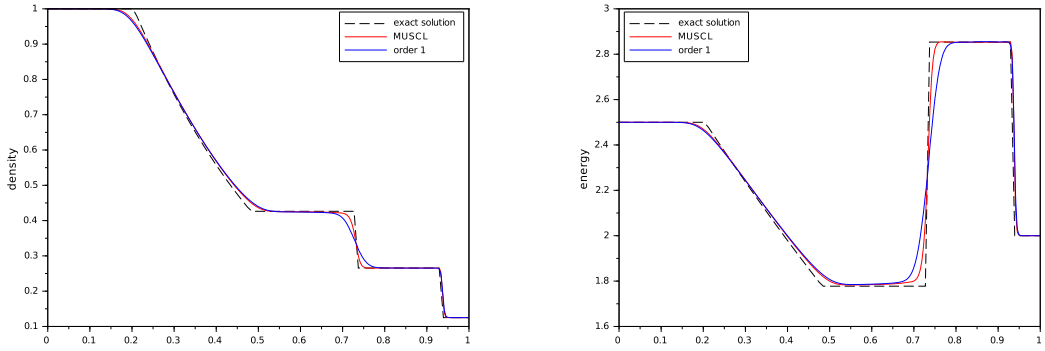

Figure 3: Density and internal energy for Test 1

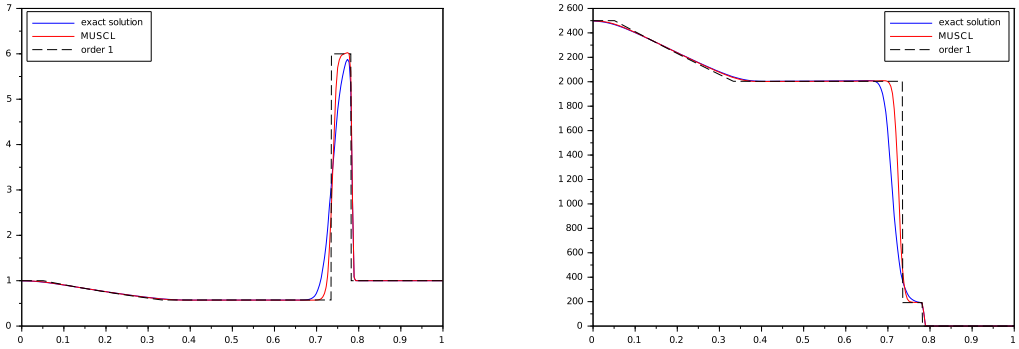

Figure 4: Density and internal energy for Test 2

We display the results of the two tests in Table 1 that both consist of a left rarefaction, a contact discontinuity and a right shock, with Test 2 being more severe. These tests are clearly

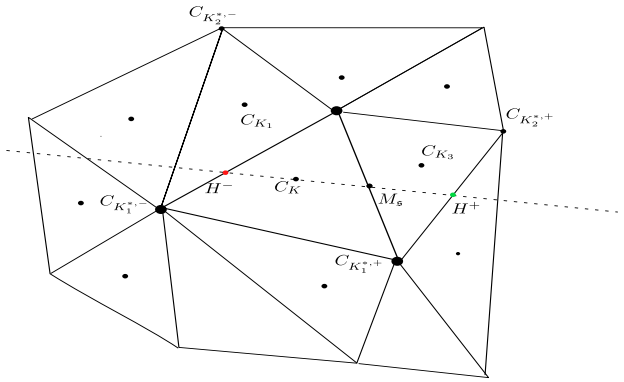

Figure 5: Forward and backward points $\mathbf{H}_{K,\sigma}^{*,-}$ and $\mathbf{H}_{K,\sigma}^{*,+}$

1D in nature; nevertheless we perform simulations with a 2D code. We see in both cases, Fig. 3 and 4 respectively, that the numerical diffusion in the density and internal energy profiles at the contact discontinuity is drastically reduced by the MUSCL approximation (the velocity being constant).

4.2 Primal and dual velocities, momentum fluxes

We turn to the reconstruction of velocities. We remind the reader that discrete velocities are stored on both the centers and vertices of the primal mesh (the latter being the centers of the dual mesh). Such a dual representation appeared in the work of C. Berthon, Y. Coudière and V. Desveaux [7], the increased degrees of freedom being used to define accurate gradients. Indeed, we can naturally use unknowns located on a grid for defining the slopes of the interpolation from the other grid. The reconstruction we adopt is inspired from [12].

Let us detail the MUSCL reconstruction for the primal velocities. The reconstructed value of the velocity on the edge σ of a cell K reads as follows

$$\mathbf{u}_{K,\sigma}^{ML} = \mathbf{u}_K + \phi(s_{K,\sigma}^-, s_{K,\sigma}^+) \cdot ||\mathbf{C}_K\mathbf{M}_{K,\sigma}||, \tag{29}$$

where $\mathbf{C}_K$ stands for the center of the primal cell K and $\mathbf{M}_{K,\sigma}$ the midpoint of the edge σ. The definition involves auxiliary velocities $\mathbf{u}_{\mathbf{H}_{K,\sigma}^{*,-}}$ and $\mathbf{u}_{\mathbf{H}_{K,\sigma}^{*,+}}$, computed on two points $\mathbf{H}_{K,\sigma}^{*,-}$ and $\mathbf{H}_{K,\sigma}^{*,+}$, so that the backward and forward slopes $s_{K,\sigma}^-$ and $s_{K,\sigma}^+$ are given by

$$s_{K,\sigma}^- = \frac{\mathbf{u}_K - \mathbf{u}_{\mathbf{H}_\sigma^{*,-}}}{||\mathbf{C}_K\mathbf{H}_{K,\sigma}^{*,-}||}, \qquad s_{K,\sigma}^+ = \frac{\mathbf{u}_{\mathbf{H}_\sigma^{*,+}} - \mathbf{u}_K}{||\mathbf{C}_K\mathbf{H}_{K,\sigma}^{*,+}||}.$$

The backward point $\mathbf{H}_{K,\sigma}^{*,-}$ is nothing but the intersection of the axis $(\mathbf{C}_K\mathbf{M}_{K,\sigma})$ with the edge, different from σ, of the cell K (see Fig. 5), The forward point $\mathbf{H}_{K,\sigma}^{*,+}$ is the intersection of $(\mathbf{C}_K\mathbf{M}_{K,\sigma})$ with the edge of the cell L that shares the edge σ with the cell K. Next, as mentioned above, we use the dual velocities defined on the vertices of these edges for defining the interpolation of $\mathbf{u}_{\mathbf{H}_{K,\sigma}^{*,-}}$ and $\mathbf{u}_{\mathbf{H}_{K,\sigma}^{*,+}}$ as follows:

$$\mathbf{u}_{\mathbf{H}_{K,\sigma}^{*,-}} = \alpha_1^- \mathbf{u}_{K_1^{*,-}} + \alpha_2^- \mathbf{u}_{K_2^{*,-}}, \quad \mathbf{u}_{\mathbf{H}_{K,\sigma}^{*,+}} = \alpha_1^+ \mathbf{u}_{K_1^{*,+}} + \alpha_2^+ \mathbf{u}_{K_2^{*,+}},$$

where

$$\alpha_1^{\pm} = \frac{||\mathbf{C}_{K_2^{*,\pm}}\mathbf{H}_{K,\sigma}^{*,\pm}||}{||\mathbf{C}_{K_1^{*,\pm}}\mathbf{C}_{K_2^{*,\pm}}||} \geq 0, \quad \alpha_2^{\pm} = \frac{||\mathbf{C}_{K_1^{*,\pm}}\mathbf{H}_{K,\sigma}^{*,\pm}||}{||\mathbf{C}_{K_1^{*,\pm}}\mathbf{C}_{K_2^{*,\pm}}||} \geq 0, \quad \alpha_1^{\pm} + \alpha_2^{\pm} = 1.$$

Again, we point out that the points $\mathbf{H}_{K,\sigma}^{*,-}$ and $\mathbf{H}_{K,\sigma}^{*,+}$ and the coefficients $\alpha_1^{\pm}$ and $\alpha_2^{\pm}$ depends on the mesh and can be computed once for all when starting the code.

Details for the dual mesh

The momentum fluxes are defined by averaging the upgraded mass fluxes $\mathcal{F}_{D_{\sigma,\sigma^*},\mathfrak{s}}^{ML,+}$ and $\mathcal{F}_{D_{\sigma,\sigma^*},\mathfrak{s}}^{ML,-}$

$$\mathcal{F}_{K,\sigma}^{ML,\pm} = \frac{|D_{\sigma,\sigma^*} \cap K|}{|D_{\sigma,\sigma^*}|} \sum_{\substack{\mathfrak{s}\in\partial D_{\sigma,\sigma^*} \\ \mathfrak{s}\subset L}} \frac{|\mathfrak{s}|}{|\sigma|} \mathcal{F}_{D_{\sigma,\sigma^*},\mathfrak{s}}^{ML,\pm} - \frac{|D_{\sigma,\sigma^*} \cap L|}{|D_{\sigma,\sigma^*}|} \sum_{\substack{\mathfrak{s}\in\partial D_{\sigma,\sigma^*} \\ \mathfrak{s}\subset K}} \frac{|\mathfrak{s}|}{|\sigma|} \mathcal{F}_{D_{\sigma,\sigma^*},\mathfrak{s}}^{ML,\pm}, \tag{30}$$

$$\mathcal{F}_{K^*,\sigma^*}^{ML,\pm} = \frac{|D_{\sigma,\sigma^*} \cap K^*|}{|D_{\sigma,\sigma^*}|} \sum_{\substack{\mathfrak{s}\in\partial D_{\sigma,\sigma^*} \\ \mathfrak{s}\subset L^*}} \frac{|\mathfrak{s}|}{|\sigma^*|} \mathcal{F}_{D_{\sigma,\sigma^*},\mathfrak{s}}^{ML,\pm} - \frac{|D_{\sigma,\sigma^*} \cap L^*|}{|D_{\sigma,\sigma^*}|} \sum_{\substack{\mathfrak{s}\in\partial D_{\sigma,\sigma^*} \\ \mathfrak{s}\subset K^*}} \frac{|\mathfrak{s}|}{|\sigma^*|} \mathcal{F}_{D_{\sigma,\sigma^*},\mathfrak{s}}^{ML,\pm}, \tag{31}$$

so that

$$\mathcal{F}_{K,\sigma}^{ML} = \mathcal{F}_{K,\sigma}^{ML,+} + \mathcal{F}_{K,\sigma}^{ML,-} \quad \text{and} \quad \mathcal{F}_{K^*,\sigma^*}^{ML} = \mathcal{F}_{K^*,\sigma^*}^{ML,+} + \mathcal{F}_{K^*,\sigma^*}^{ML,-}$$

Observe that the averaged densities ρ_K, ρ_{K^*} satisfy the discrete conservation law

$$|K|\frac{\overline{\rho}_K - \rho_K}{\delta t} + \sum_{D_{\sigma,\sigma^*}\in\mathfrak{D}_K} |\sigma| \mathcal{F}_{K,\sigma}^{ML} = 0, \tag{32}$$

$$|K^*|\frac{\overline{\rho}_{K^*} - \rho_{K^*}}{\delta t} + \sum_{D_{\sigma,\sigma^*}\in\mathfrak{D}_{K^*}} |\sigma^*| \mathcal{F}_{K^*,\sigma^*}^{ML} + \sum_{D_{\sigma,\sigma^*}\in\mathfrak{D}_{K^*}\cap\mathfrak{D}_{ext}} \frac{|\sigma|}{2} \mathcal{F}_{\sigma}^{ML} = 0. \tag{33}$$

These equalities can be obtained by reproducing the arguments for [29, Proposition 3.5]. Finally, the momentum fluxes are defined as follows:

$$\mathcal{G}_{K,\sigma}^{ML} = \mathcal{F}_{K,\sigma}^{ML,+}\mathbf{u}_{K,\sigma}^{ML} + \mathcal{F}_{K,\sigma}^{ML,-}\mathbf{u}_{L,\sigma}^{ML} \quad \text{and} \quad \mathcal{G}_{K^*,\sigma^*}^{ML} = \mathcal{F}_{K^*,\sigma^*}^{ML,+}\mathbf{u}_{K^*,\sigma^*}^{ML} + \mathcal{F}_{K^*,\sigma^*}^{ML,-}\mathbf{u}_{L^*,\sigma^*}^{ML}.$$

a few words about the pressure gradient ?

4.3 Internal energy balance

We have already described the derivation of the numerical fluxes for the internal energy equation. However, the update of the internal energy also involves correction terms coming form the kinetic energy balance, which thus need to take into account the modification of the momentum fluxes.

a few words about the pdiv(u) term ?

Firs, let us introduce the new kinetic energy fluxes $\mathcal{K}_{K,\sigma}^{ML}$ from primal cells and $\mathcal{K}_{K^*,\sigma^*}^{ML}$ from dual cells. For $\sigma \not\subset \partial\Omega$, we set

$$\mathcal{K}_{K,\sigma}^{ML} = \mathcal{F}_{K,\sigma}^{ML,+}\frac{\|\mathbf{u}_K^{ML}\|^2}{2} + \mathcal{F}_{K,\sigma}^{ML,-}\frac{\|\mathbf{u}_L^{ML}\|^2}{2}, \quad \text{and} \quad \mathcal{K}_{K^*,\sigma^*}^{ML} = \mathcal{F}_{K^*,\sigma^*}^{ML,+}\frac{\|\mathbf{u}_{K^*}^{ML}\|^2}{2} + \mathcal{F}_{K^*,\sigma^*}^{ML,-}\frac{\|\mathbf{u}_{L^*}^{ML}\|^2}{2}. \tag{34}$$

For the boundary terms, when $\sigma \subset \partial\Omega$, we set

$$\mathcal{K}_{K,\sigma}^{ML} = \mathcal{F}_{\sigma}^{ML,+}\frac{\|\mathbf{u}_K^{ML}\|^2}{2} + \mathcal{F}_{\sigma}^{ML,-}\frac{\|\mathbf{u}_\sigma\|^2}{2} \quad \text{and} \quad \mathcal{K}_{K^*,\sigma}^{ML} = \mathcal{F}_{\sigma}^{ML,+}\frac{\|\mathbf{u}_{K^*}^{ML}\|^2}{2} + \mathcal{F}_{\sigma}^{ML,-}\frac{\|\mathbf{u}_\sigma\|^2}{2}.$$

Next, we define the remainder terms. For $K \in \mathfrak{M}$ we set

$$\mathcal{R}_K^{ML} = \frac{\overline{\rho}_K}{2\delta t}\|\overline{\mathbf{u}}_K - \mathbf{u}_K\|^2 + \frac{1}{|K|}\sum_{D_{\sigma,\sigma^*}\in\mathfrak{D}_K} |\sigma|\Bigg[\mathcal{F}_{K,\sigma}^{ML,+}\left(\frac{\|\overline{\mathbf{u}}_K - \mathbf{u}_K\|^2}{2} - \frac{\|\overline{\mathbf{u}}_K - \mathbf{u}_K^{ML}\|^2}{2}\right) + \mathcal{F}_{K,\sigma}^{ML,-}\left(\frac{\|\overline{\mathbf{u}}_K - \mathbf{u}_K\|^2}{2} - \frac{\|\overline{\mathbf{u}}_K - \mathbf{u}_L^{ML}\|^2}{2}\right)\Bigg]$$

with the convention that $\mathbf{u}_L = \mathbf{u}_\sigma$ when $\sigma \subset \partial\Omega$. For $K^* \in \mathfrak{M}^* \cup \partial\mathfrak{M}^*$, we set

$$\begin{aligned}\mathcal{R}_{K^*}^{ML} = \frac{\overline{\rho}_{K^*}}{2\delta t}\|\overline{\mathbf{u}}_{K^*} - \mathbf{u}_{K^*}\|^2 &+ \frac{1}{|K^*|}\sum_{D_{\sigma,\sigma^*}\in\mathfrak{D}_{K^*}} |\sigma^*|\Bigg[\mathcal{F}_{K^*,\sigma^*}^{ML,+}\left(\frac{\|\overline{\mathbf{u}}_{K^*} - \mathbf{u}_{K^*}\|^2}{2} - \frac{\|\overline{\mathbf{u}}_{K^*} - \mathbf{u}_{K^*}^{ML}\|^2}{2}\right)\\ &+ \mathcal{F}_{K^*,\sigma^*}^{ML,-}\left(\frac{\|\overline{\mathbf{u}}_{K^*} - \mathbf{u}_{K^*}\|^2}{2} - \frac{\|\overline{\mathbf{u}}_{K^*} - \mathbf{u}_{L^*}^{ML}\|^2}{2}\right)\Bigg]\\ &+ \frac{1}{|K^*|}\sum_{D_{\sigma,\sigma^*}\in\mathfrak{D}_{K^*}\cap\mathfrak{D}_{ext}} \frac{|\sigma|}{2}\Bigg[\mathcal{F}_{\sigma}^{ML,+}\left(\frac{\|\overline{\mathbf{u}}_{K^*} - \mathbf{u}_{K^*}\|^2}{2} - \frac{\|\overline{\mathbf{u}}_{K^*} - \mathbf{u}_{K^*}^{ML}\|^2}{2}\right)\\ &+ \mathcal{F}_{\sigma}^{ML,-}\left(\frac{\|\overline{\mathbf{u}}_{K^*} - \mathbf{u}_{K^*}\|^2}{2} - \frac{\|\overline{\mathbf{u}}_{K^*} - \mathbf{u}_{\sigma}\|^2}{2}\right)\Bigg].\end{aligned}$$

With these definitions we obtain the following expression for the balance of kinetic energy.

Lemma 4.1. *For $K \in \mathfrak{M}$ and $K^* \in \mathfrak{M}^* \cup \partial\mathfrak{M}^*$, we have*

$$\frac{\overline{\rho}_K\dfrac{\|\overline{\mathbf{u}}_K\|^2}{2} - \rho_K\dfrac{\|\mathbf{u}_K\|^2}{2}}{\delta t} + \frac{1}{|K|}\sum_{D_{\sigma,\sigma^*}\in\mathfrak{D}_K} |\sigma|\mathcal{K}_{K,\sigma}^{ML} + (\boldsymbol{\nabla_d} p)_K \cdot \overline{\mathbf{u}}_K = -\mathcal{R}_K^{ML}. \tag{35}$$

$$\begin{aligned}&\frac{\overline{\rho}_{K^*}\dfrac{\|\overline{\mathbf{u}}_{K^*}\|^2}{2} - \rho_{K^*}\dfrac{\|\mathbf{u}_{K^*}\|^2}{2}}{\delta t} + \frac{1}{|K^*|}\sum_{D_{\sigma,\sigma^*}\in\mathfrak{D}_{K^*}} |\sigma^*|\mathcal{K}_{K^*,\sigma^*}^{ML}\\ &\qquad + \frac{1}{|K^*|}\sum_{D_{\sigma,\sigma^*}\in\mathfrak{D}_{K^*}\cap\mathfrak{D}_{ext}} \frac{|\sigma|}{2}\mathcal{K}_{K^*,\sigma}^{ML} + (\boldsymbol{\nabla_d} p)_{K^*} \cdot \overline{\mathbf{u}}_{K^*} = -\mathcal{R}_{K^*}^{ML}.\end{aligned} \tag{36}$$

Proof. For $X \in \mathfrak{T}$, we multiply by $\overline{\mathbf{u}}_X$ the momentum equation (14) and use the averaged mass equation (32).

a) Let $K \in \mathfrak{M}$. In what follows, we use the convention that $\mathbf{u}_L = \mathbf{u}_\sigma$ when the edge $\sigma \subset \partial\Omega$. We start by remarking that

$$\begin{aligned}\frac{\overline{\rho}_K\overline{\mathbf{u}}_K - \rho_K\mathbf{u}_K}{\delta t}\cdot\overline{\mathbf{u}}_K =& \frac{1}{\delta t}\left(\overline{\rho}_K\frac{\|\overline{\mathbf{u}}_K\|^2}{2} - \rho_K\frac{\|\mathbf{u}_K\|^2}{2} + \frac{\overline{\rho}_K}{2}\|\overline{\mathbf{u}}_K - \mathbf{u}_K\|^2\right)\\ &- \frac{\overline{\rho}_K - \rho_K}{\delta t}\left(\frac{\|\mathbf{u}_K\|^2}{2} - \mathbf{u}_K\cdot\overline{\mathbf{u}}_K\right).\end{aligned}$$

Thus, using the average mass balance (32) we get

$$\begin{aligned}\frac{\overline{\rho}_K\overline{\mathbf{u}}_K - \rho_K\mathbf{u}_K}{\delta t}\cdot\overline{\mathbf{u}}_K =& \frac{1}{\delta t}\left(\overline{\rho}_K\frac{\|\overline{\mathbf{u}}_K\|^2}{2} - \rho_K\frac{\|\mathbf{u}_K\|^2}{2} + \frac{\overline{\rho}_K}{2}\|\overline{\mathbf{u}}_K - \mathbf{u}_K\|^2\right)\\ &+ \frac{1}{|K|}\sum_{D_{\sigma,\sigma^*}\in\mathfrak{D}_K} |\sigma|\mathcal{F}_{K,\sigma}^{ML}\left(\frac{\|\mathbf{u}_K\|^2}{2} - \mathbf{u}_K\cdot\overline{\mathbf{u}}_K\right).\end{aligned}$$

It is convenient to introduce the notation

$$\mathcal{F}^{|\cdot|} = \mathcal{F}^+ - \mathcal{F}^-.$$

We bear in mind that $\mathcal{F} = \mathcal{F}^+ + \mathcal{F}^-$. Hence, the momentum fluxes can be recast as

$$\mathcal{G}_{K,\sigma}^{ML} = \frac{\mathcal{F}_{K,\sigma}^{ML,|\cdot|} + \mathcal{F}_{K,\sigma}^{ML}}{2}\mathbf{u}_K^{ML} + \frac{\mathcal{F}_{K,\sigma}^{ML} - \mathcal{F}_{K,\sigma}^{ML,|\cdot|}}{2}\mathbf{u}_L^{ML} = \mathcal{F}_{K,\sigma}^{ML}\frac{\mathbf{u}_K^{ML} + \mathbf{u}_L^{ML}}{2} + \mathcal{F}_{K,\sigma}^{ML,|\cdot|}\frac{\mathbf{u}_K^{ML} - \mathbf{u}_L^{ML}}{2}.$$

We also remind the reader the conservation equations:

$$|K|\frac{\overline{\rho}_K - \rho_K}{\delta t} + \sum_{D_{\sigma,\sigma^*} \in \mathfrak{D}_K} |\sigma| \mathcal{F}_{K,\sigma} = 0,$$

$$|K^*|\frac{\overline{\rho}_{K^*} - \rho_{K^*}}{\delta t} + \sum_{D_{\sigma,\sigma^*} \in \mathfrak{D}_{K^*}} |\sigma^*| \mathcal{F}_{K^*,\sigma^*} + \sum_{D_{\sigma,\sigma^*} \in \mathfrak{D}_{K^*} \cap \mathfrak{D}_{ext}} \frac{|\sigma|}{2}\mathcal{F}_\sigma = 0.$$

We obtain

$$\frac{\overline{\rho}_K \dfrac{\|\overline{\mathbf{u}}_K\|^2}{2} - \rho_K \dfrac{\|\mathbf{u}_K\|^2}{2}}{\delta t} + \frac{\overline{\rho}_K}{2\delta t}\|\overline{\mathbf{u}}_K - \mathbf{u}_K\|^2 + (\boldsymbol{\nabla}_{\boldsymbol{d}} p)_K \cdot \overline{\mathbf{u}}_K + \frac{1}{|K|}\sum_{D_{\sigma,\sigma^*} \in \mathfrak{D}_K} |\sigma| B_{K,\sigma}^{ML} = 0, \quad (37)$$

where

$$\begin{aligned}
B_{K,\sigma}^{ML} &= \mathcal{F}_{K,\sigma}^{ML}\left(\frac{\|\mathbf{u}_K\|^2}{2} - \mathbf{u}_K \cdot \overline{\mathbf{u}}_K + \frac{\mathbf{u}_K^{ML} + \mathbf{u}_L^{ML}}{2} \cdot \overline{\mathbf{u}}_K\right) + \mathcal{F}_{K,\sigma}^{ML,|\cdot|}\frac{\mathbf{u}_K^{ML} - \mathbf{u}_L^{ML}}{2} \cdot \overline{\mathbf{u}}_K \\
&= \mathcal{F}_{K,\sigma}^{ML}\left(\frac{\|\mathbf{u}_K\|^2}{2} + (\mathbf{u}_K^{ML} - \mathbf{u}_K) \cdot \overline{\mathbf{u}}_K - \frac{\mathbf{u}_K^{ML} - \mathbf{u}_L^{ML}}{2} \cdot \overline{\mathbf{u}}_K\right) + \mathcal{F}_{K,\sigma}^{ML,|\cdot|}\frac{\mathbf{u}_K^{ML} - \mathbf{u}_L^{ML}}{2} \cdot \overline{\mathbf{u}}_K \\
&= \mathcal{F}_{K,\sigma}^{ML}\left(\frac{\|\mathbf{u}_K\|^2}{2} + (\mathbf{u}_K^{ML} - \mathbf{u}_K) \cdot \overline{\mathbf{u}}_K\right) - \mathcal{F}_{K,\sigma}^{ML,-}(\mathbf{u}_K^{ML} - \mathbf{u}_L^{ML}) \cdot \overline{\mathbf{u}}_K \\
&= \left(\mathcal{F}_{K,\sigma}^{ML,+}\frac{\|\mathbf{u}_K^{ML}\|^2}{2} + \mathcal{F}_{K,\sigma}^{ML,-}\frac{\|\mathbf{u}_L^{ML}\|^2}{2}\right) + \mathcal{F}_{K,\sigma}^{ML,+}\left(\frac{\|\mathbf{u}_K\|^2}{2} - \frac{\|\mathbf{u}_K^{ML}\|^2}{2}\right) \\
&\quad + \mathcal{F}_{K,\sigma}^{ML,-}\left(\frac{\|\mathbf{u}_K\|^2}{2} - \frac{\|\mathbf{u}_L^{ML}\|^2}{2} - (\mathbf{u}_K^{ML} - \mathbf{u}_L^{ML}) \cdot \overline{\mathbf{u}}_K\right) + \mathcal{F}_{K,\sigma}^{ML}(\mathbf{u}_K^{ML} - \mathbf{u}_K) \cdot \overline{\mathbf{u}}_K \\
&= \mathcal{K}_{K,\sigma}^{ML} + \mathcal{F}_{K,\sigma}^{ML,+}\left(\frac{\|\mathbf{u}_K\|^2}{2} - \frac{\|\mathbf{u}_K^{ML}\|^2}{2} - (\mathbf{u}_K - \mathbf{u}_K^{ML}) \cdot \overline{\mathbf{u}}_K\right) \\
&\quad + \mathcal{F}_{K,\sigma}^{ML,-}\left(\frac{\|\mathbf{u}_K\|^2}{2} - \frac{\|\mathbf{u}_L^{ML}\|^2}{2} - (\mathbf{u}_K - \mathbf{u}_L^{ML}) \cdot \overline{\mathbf{u}}_K\right) \\
&= \mathcal{K}_{K,\sigma}^{ML} + \mathcal{F}_{K,\sigma}^{ML,+}\left(\frac{\|\overline{\mathbf{u}}_K - \mathbf{u}_K\|^2}{2} - \frac{\|\overline{\mathbf{u}}_K - \mathbf{u}_K^{ML}\|^2}{2}\right) \\
&\quad + \mathcal{F}_{K,\sigma}^{ML,-}\left(\frac{\|\overline{\mathbf{u}}_K - \mathbf{u}_K\|^2}{2} - \frac{\|\overline{\mathbf{u}}_K - \mathbf{u}_L^{ML}\|^2}{2}\right)
\end{aligned}$$

Coming back to (37), we arrive at (35).

b) For $K^* \in \mathfrak{M}^* \cup \partial\mathfrak{M}^*$, we start by remarking that

$$\begin{aligned}
\frac{\overline{\rho}_{K^*}\overline{\mathbf{u}}_{K^*} - \rho_{K^*}\mathbf{u}_{K^*}}{\delta t} \cdot \overline{\mathbf{u}}_{K^*} = &\frac{1}{\delta t}\left(\overline{\rho}_{K^*}\frac{\|\overline{\mathbf{u}}_{K^*}\|^2}{2} - \rho_{K^*}\frac{\|\mathbf{u}_{K^*}\|^2}{2} + \frac{\overline{\rho}_{K^*}}{2}\|\overline{\mathbf{u}}_{K^*} - \mathbf{u}_{K^*}\|^2\right) \\
&- \frac{\overline{\rho}_{K^*} - \rho_{K^*}}{\delta t}\left(\frac{\|\mathbf{u}_{K^*}\|^2}{2} - \mathbf{u}_{K^*} \cdot \overline{\mathbf{u}}_{K^*}\right).
\end{aligned}$$

Thus, using the averaged mass balance (33) we get

$$\begin{aligned}\frac{\overline{\rho}_{K^*}\overline{\mathbf{u}}_{K^*}-\rho_{K^*}\mathbf{u}_{K^*}}{\delta t}\cdot\overline{\mathbf{u}}_{K^*} =&\frac{1}{\delta t}\left(\overline{\rho}_{K^*}\frac{\|\overline{\mathbf{u}}_{K^*}\|^2}{2}-\rho_{K^*}\frac{\|\mathbf{u}_{K^*}\|^2}{2}+\frac{\overline{\rho}_{K^*}}{2}\|\overline{\mathbf{u}}_{K^*}-\mathbf{u}_{K^*}\|^2\right)\\ &+\frac{1}{|K^*|}\sum_{D_{\sigma,\sigma^*}\in\mathfrak{D}_{K^*}}|\sigma^*|\mathcal{F}^{ML}_{K^*,\sigma^*}\left(\frac{\|\mathbf{u}_{K^*}\|^2}{2}-\mathbf{u}_{K^*}\cdot\overline{\mathbf{u}}_{K^*}\right)\\ &+\frac{1}{|K^*|}\sum_{D_{\sigma,\sigma^*}\in\mathfrak{D}_{K^*}\cap\mathfrak{D}_{ext}}\frac{|\sigma|}{2}\mathcal{F}^{ML}_{K^*,\sigma}\left(\frac{\|\mathbf{u}_{K^*}\|^2}{2}-\mathbf{u}_{K^*}\cdot\overline{\mathbf{u}}_{K^*}\right).\end{aligned}$$

The momentum equation multiplied by $\overline{\mathbf{u}}_{K^*}$ becomes

$$\begin{aligned}&\frac{\overline{\rho}_{K^*}\frac{\|\overline{\mathbf{u}}_{K^*}\|^2}{2}-\rho_{K^*}\frac{\|\mathbf{u}_{K^*}\|^2}{2}}{\delta t}+\frac{\overline{\rho}_{K^*}}{2\delta t}\|\overline{\mathbf{u}}_{K^*}-\mathbf{u}_{K^*}\|^2+(\boldsymbol{\nabla_d} p)_{K^*}\cdot\overline{\mathbf{u}}_{K^*}\\ &\quad+\frac{1}{|K^*|}\left(\sum_{D_{\sigma,\sigma^*}\in\mathfrak{D}_{K^*}}|\sigma^*|\mathcal{F}^{ML}_{K^*,\sigma^*}+\sum_{D_{\sigma,\sigma^*}\in\mathfrak{D}_{K^*}\cap\mathfrak{D}_{ext}}\frac{|\sigma|}{2}\mathcal{F}^{ML}_{\sigma}\right)\left(\frac{\|\mathbf{u}_{K^*}\|^2}{2}-\mathbf{u}_{K^*}\cdot\overline{\mathbf{u}}_{K^*}\right)\\ &\quad+\frac{1}{|K^*|}\left(\sum_{D_{\sigma,\sigma^*}\in\mathfrak{D}_{K^*}}|\sigma^*|\mathcal{G}^{ML}_{K^*,\sigma^*}+\sum_{D_{\sigma,\sigma^*}\in\mathfrak{D}_{K^*}\cap\mathfrak{D}_{ext}}\frac{|\sigma|}{2}\mathcal{G}^{ML}_{K^*,\sigma}\right)\cdot\overline{\mathbf{u}}_{K^*}=0.\end{aligned}$$

We obtain (36) by remarking that, for any $D_{\sigma,\sigma^*}\in\mathfrak{D}_{K^*}$,

$$\begin{aligned}&\mathcal{F}^{ML}_{K^*,\sigma^*}\left(\frac{\|\mathbf{u}_{K^*}\|^2}{2}-\mathbf{u}_{K^*}\cdot\overline{\mathbf{u}}_{K^*}\right)+\mathcal{G}^{ML}_{K^*,\sigma^*}\cdot\overline{\mathbf{u}}_{K^*}\\ &\qquad=\mathcal{K}^{ML}_{K^*,\sigma^*}+\mathcal{F}^{ML,+}_{K^*,\sigma^*}\left(\frac{\|\overline{\mathbf{u}}_{K^*}-\mathbf{u}_{K^*}\|^2}{2}-\frac{\|\overline{\mathbf{u}}_{K^*}-\mathbf{u}^{ML}_{K^*}\|^2}{2}\right)\\ &\qquad\quad+\mathcal{F}^{ML,-}_{K^*,\sigma^*}\left(\frac{\|\overline{\mathbf{u}}_{K^*}-\mathbf{u}_{K^*}\|^2}{2}-\frac{\|\overline{\mathbf{u}}_{K^*}-\mathbf{u}^{ML}_{L^*}\|^2}{2}\right)\end{aligned}$$

and similarly, for any $D_{\sigma,\sigma^*}\in\mathfrak{D}_{K^*}\cap\mathfrak{D}_{ext}$, there holds

$$\begin{aligned}&\mathcal{F}^{ML}_{\sigma}\left(\frac{\|\mathbf{u}_{K^*}\|^2}{2}-\mathbf{u}_{K^*}\cdot\overline{\mathbf{u}}_{K^*}\right)+\mathcal{G}^{ML}_{K^*,\sigma}\cdot\overline{\mathbf{u}}_{K^*}\\ &\qquad=\mathcal{K}^{ML}_{K^*,\sigma}+\mathcal{F}^{ML,+}_{\sigma}\left(\frac{\|\overline{\mathbf{u}}_{K^*}-\mathbf{u}_{K^*}\|^2}{2}-\frac{\|\overline{\mathbf{u}}_{K^*}-\mathbf{u}^{ML}_{K^*}\|^2}{2}\right)\\ &\qquad\quad+\mathcal{F}^{ML,-}_{\sigma}\left(\frac{\|\overline{\mathbf{u}}_{K^*}-\mathbf{u}_{K^*}\|^2}{2}-\frac{\|\overline{\mathbf{u}}_{K^*}-\mathbf{u}_{\sigma}\|^2}{2}\right).\end{aligned}$$

■

4.3.1 Stability: positivity of the density

We are going to prove that the MUSCL reconstruction preserves the non negativity of the density, up to a strengthened constraint on the time step, compared to Proposition 4.2 for the first order scheme. and the internal energy.

Proposition 4.2. *Let $\rho_{\sigma,\sigma^*} \geqslant 0$. We assume that the following CFL-like conditions are satisfied*

$$\frac{\delta t}{|D_{\sigma,\sigma^*}|} \sum_{\mathfrak{s}\in\partial D_{\sigma,\sigma^*}} |\mathfrak{s}|[\lambda_+(c(e^{ML}_{D_{\sigma,\sigma^*},\mathfrak{s}}), u_{D_{\sigma,\sigma^*},\mathfrak{s}})]^+ \leqslant \frac{1}{3}, \qquad \forall D_{\sigma,\sigma^*} \in \mathfrak{D}_{int}$$
$$\frac{\delta t}{|D_{\sigma,\sigma^*}|}\left[\sum_{\mathfrak{s}\in\partial D_{\sigma,\sigma^*}\setminus\partial\Omega} |\mathfrak{s}|[\lambda_+(c(e^{ML}_{D_{\sigma,\sigma^*},\mathfrak{s}}), u_{D_{\sigma,\sigma^*},\mathfrak{s}})]^+ + |\sigma|[\lambda_+(c(e_\sigma), u_\sigma)]^+\right] \leqslant \frac{1}{3}, \qquad \forall D_{\sigma,\sigma^*} \in \mathfrak{D}_{ext}. \tag{38}$$

Then, the non negativity of the density ρ_{σ,σ^*} is preserved: $\overline{\rho}_{\sigma,\sigma^*} \geqslant 0$.

Proof. The proof uses properties that should be fulfilled by the flux limiter ϕ, see [47]. It is convenient to rewrite the limiter as a function of a single variable

$$\phi(a,b) = b\ \hat{\phi}(\frac{a}{b}) = a\ \hat{\phi}(\frac{b}{a}) = \phi(b,a) \tag{39}$$

where it is understood that the function $\hat{\phi}$ satisfies the symmetry property

$$\hat{\phi}(r) = \hat{\phi}\left(\frac{1}{r}\right), \quad \forall r \neq 0.$$

The limiter function $\hat{\phi}$ is required to lie in the Sweeby region, see [47], characterized by the inequalities

$$\hat{\phi}(r) = 0, \forall r \neq 0, \qquad 0 \leq \left(\hat{\phi}(r), \frac{\hat{\phi}(r)}{r}\right) \leq 2, \forall r \geq 0.$$

Let

$$\alpha_{D_{\sigma,\sigma^*},\mathfrak{s}} = \frac{||\mathbf{C}_{D_{\sigma,\sigma^*}}\mathbf{M}_\mathfrak{s}||}{||\mathbf{C}_{D_{\sigma,\sigma^*}}\mathbf{H}^-_\mathfrak{s}||}\ \hat{\phi}\left(\frac{\rho_{\mathbf{H}^+_\mathfrak{s}} - \rho_{\sigma,\sigma^*}}{||\mathbf{C}_{D_{\sigma,\sigma^*}}\mathbf{H}^+_\mathfrak{s}||}\ \frac{||\mathbf{C}_{D_{\sigma,\sigma^*}}\mathbf{H}^-_\mathfrak{s}||}{\rho_{\sigma,\sigma^*} - \rho_{\mathbf{H}^-_\mathfrak{s}}}\right),$$

so that

$$\rho^{ML}_{D_{\sigma,\sigma^*},\mathfrak{s}} = (1 + \alpha_{D_{\sigma,\sigma^*},\mathfrak{s}})\rho_{\sigma,\sigma^*} - \alpha_{D_{\sigma,\sigma^*},\mathfrak{s}}\ \rho_{\mathbf{H}^-_\mathfrak{s}}.$$

Since $\hat{\phi}(r) \leq 2$, we deduce that $\rho^{ML}_{D_{\sigma,\sigma^*},\mathfrak{s}} \leq 3\rho_{\sigma,\sigma^*}$. By construction of the point $\mathbf{H}^-_\mathfrak{s}$, we always have $||\mathbf{C}_{D_{\sigma,\sigma^*}}\mathbf{M}_\mathfrak{s}|| \leq ||\mathbf{C}_{D_{\sigma,\sigma^*}}\mathbf{H}^-_\mathfrak{s}||$.

Consider $D_{\sigma,\sigma^*} \in \mathfrak{D}_{int}$. Going back to the mass conservation equation (8) and using the properties of the flux function collected in (6), we are led to

$$\begin{aligned}
\overline{\rho}_{\sigma,\sigma^*} &= \rho_{\sigma,\sigma^*} - \frac{\delta t}{|D_{\sigma,\sigma^*}|} \sum_{\mathfrak{s}\in\partial D_{\sigma,\sigma^*}} |\mathfrak{s}|\left(\mathcal{F}^+(\rho^{ML}_{D_{\sigma,\sigma^*},\mathfrak{s}}, c(e^{ML}_{D_{\sigma,\sigma^*},\mathfrak{s}})u_{D_{\sigma,\sigma^*},\mathfrak{s}})\right. \\
&\qquad\qquad \left. + \mathcal{F}^-(\rho^{ML}_{D_{\sigma',\sigma^{*\prime}},\mathfrak{s}}, c(e^{ML}_{D_{\sigma,\sigma^*},\mathfrak{s}}), u_{D_{\sigma,\sigma^*},\mathfrak{s}})\right) \\
&\geqslant \rho_{\sigma,\sigma^*} - \frac{\delta t}{|D_{\sigma,\sigma^*}|} \sum_{\mathfrak{s}\in\partial D_{\sigma,\sigma^*}} |\mathfrak{s}|\mathcal{F}^+(\rho^{ML}_{D_{\sigma,\sigma^*},\mathfrak{s}}, c(e^{ML}_{D_{\sigma,\sigma^*},\mathfrak{s}}), u_{D_{\sigma,\sigma^*},\mathfrak{s}}) \\
&\geqslant \rho_{\sigma,\sigma^*} - \frac{\delta t}{|D_{\sigma,\sigma^*}|} \sum_{\mathfrak{s}\in\partial D_{\sigma,\sigma^*}} |\mathfrak{s}|\rho^{ML}_{D_{\sigma,\sigma^*},\mathfrak{s}}[\lambda_+(c(e^{ML}_{D_{\sigma,\sigma^*},\mathfrak{s}}), u_{D_{\sigma,\sigma^*},\mathfrak{s}})]^+ \\
&\geqslant \rho_{\sigma,\sigma^*} - \frac{\delta t}{|D_{\sigma,\sigma^*}|} \sum_{\mathfrak{s}\in\partial D_{\sigma,\sigma^*}} 3|\mathfrak{s}|\rho_{\sigma,\sigma^*}[\lambda_+(c(e^{ML}_{D_{\sigma,\sigma^*},\mathfrak{s}}), u_{D_{\sigma,\sigma^*},\mathfrak{s}})]^+.
\end{aligned}$$

With $\rho_{\sigma,\sigma^*} \geqslant 0$, the right hand side of this inequality remains non negative under the CFL-like condition (38). The proof for $D_{\sigma,\sigma^*} \in \mathfrak{D}_{ext}$ follows exactly the same lines and is left to the reader. ∎

5 Numerical results

5.1 Accuracy of the reconstruction

To check the accuracy of the method, we consider a simple advection equation for each variable. Due to the limitation procedure, we do not expect to achieve the second order exactly.

We consider first an advection equation for the density, keeping the velocity and the internal energy constant, $\mathbf{u} = (1, 0)$ and $e = 1$. The domain is $[0, 1] \times [0, 0.02]$, which is a fake two dimensional domain. The test is only intended to test the validity of the reconstruction. The equation thus reads

$$\partial_t \rho + \partial_x \rho = 0$$

with initial density $\rho_0(x) = 1 + \exp\left(-100(x - 0.4)^2\right)$. The exact solution reads $\rho(t, x) = 1 + \exp\left(-100(x - t - 0.4)^2\right)$. Next, we check the convergence order for the internal energy. We set $\rho_0(x) = 1 + \exp\left(-100(x - 0.4)^2\right)$, $e_0(x) = \frac{1+\exp\left(-200(x-0.4)^2\right)}{1+\exp(-100(x-0.4)^2)}$, and we impose $\mathbf{u} = (1, 0)$. Hence, ρe satisfies the mere transport equation

$$\partial_t \rho e + \partial_x \rho e = 0$$

with $(\rho e)_0 = 1+\exp\left(-200(x - 0.4)^2\right)$. The exact solution for the energy is $e(t, x) = \frac{1+\exp\left(-200(x-t-0.4)^2\right)}{1+\exp(-100(x-t-0.4)^2)}$. The slopes of the $L1$-error of the density and the internal energy are displayed in Fig 6: we observe the expected first and second order accuracy.

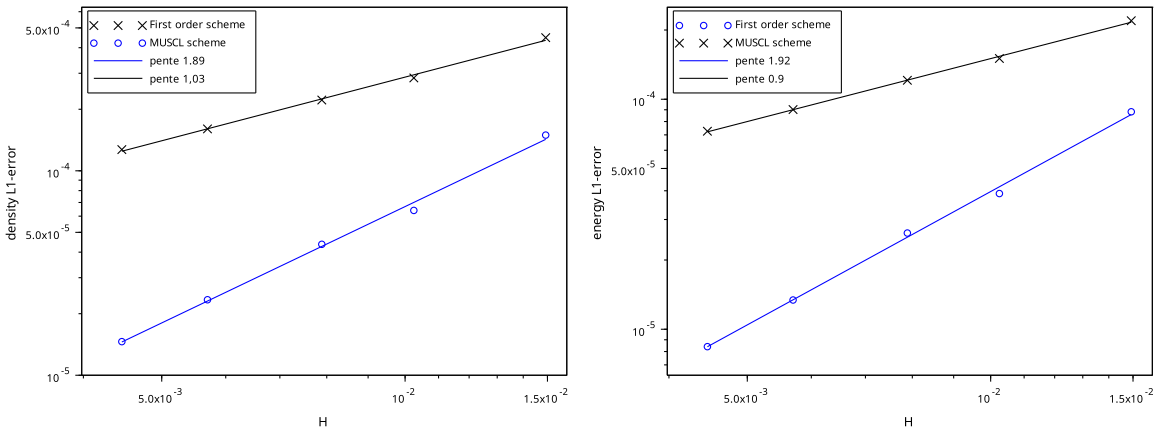

Figure 6: $L1-$error of the density (on the left) and the internal energy (on the right).

Finally, we also test the scheme for the velocity. We force the density and the internal energy to be constant, and we set $\mathbf{u}_0(x) = \left(\exp\left(-100(x - 0.4)^2\right), 0\right)$ as the initial velocity. The numerical mass fluxes boils down to correspond to a discrete transport equation for the velocity on the primal and dual cells. In other words, we need the momentum flux outgoing from a primal cell K to verify

$$\int_\sigma \mathbf{u}_K \cdot \mathbf{n}_{K,\sigma} = |\sigma| \mathcal{G}_{K,\sigma},$$

which means that the averaged mass flux $\mathcal{F}_{K,\sigma}$ equals $\mathbf{n}_{K,\sigma}$. The same idea is applied for the dual cells. The slopes are illustrated in Fig. 7. Again, we observe the expected first and second order accuracy.

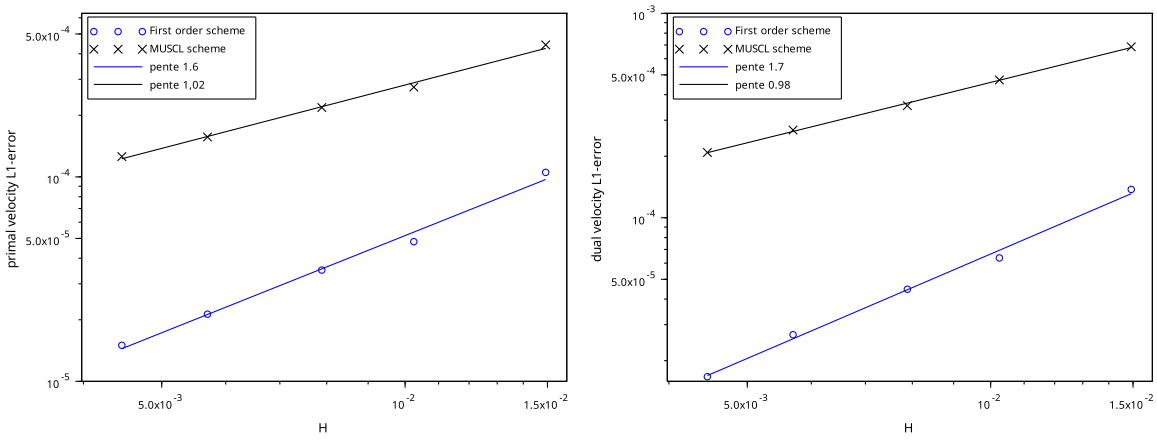

Figure 7: $L1-$error of the primal (on the left) and dual (on the right) velocity.

5.2 2d Numerical simulations

5.2.1 2d falling water columns

This test case is inspired from [1]: we consider the 2D simulation of three falling columns into a rectangular basin. The computational domain is the two-dimensional square $[-1,1]\times[-1,1]$. We assume the initial temperature (equivalently the internal energy e) is constant in the basin and we take $\gamma = 2$. The PDE system is endowed with zero-flux boundary conditions and with the following initial data

$$\begin{cases} \rho(0,x,y) = 3 + \mathbb{1}_{(x-0.5)^2+(y-0.5)^2<(0.15)^2} + \mathbb{1}_{(x+0.5)^2+(y+0.5)^2<(0.15)^2} + 2\cdot\mathbf{1}_{x^2+y^2<(0.2)^2} \\ u(0,x,y) = 0, \\ v(0,x,y) = 0. \end{cases}$$

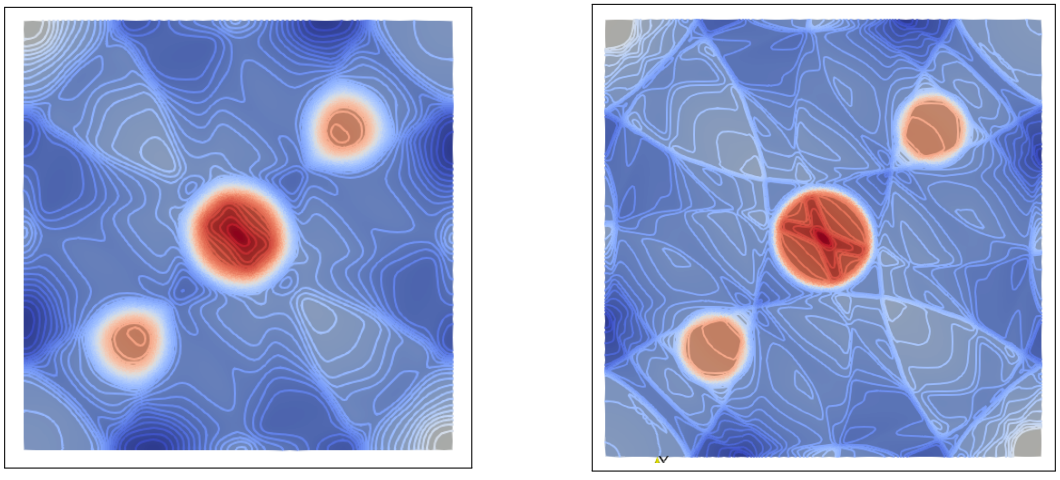

Figure 8: Density for the first order scheme (left) and MUSCL scheme (right)

.

Fig. 8 compares density contours obtained with the first order scheme (on the left) and the MUSCL scheme (on the right) with 50 contour lines. The simulation is performed on a 512×512 unstructured mesh and we choose the MinMod limiter as the flux limiter. The final time is $T = 1.035$ and the time step is $\delta t = 10^{-4}$. The MUSCL scheme shows a better resolution of the complex structures of the flow.

5.2.2 2d Mach 3 wind tunnel with a step

Next, we challenge the scheme with the 2D Mach 3 wind tunnel with a step, introduced in [53]. We set $\gamma = 1.4$. The computational domain Ω is the L-shaped domain

$$\Omega = \Omega_0 \setminus \Omega_{\text{step}}, \quad \Omega_0 = [0,3] \times [0,1], \quad \Omega_{\text{step}} = [0.6,3] \times [0,0.2].$$

We perform the simulation with a 960×320 unstructured grid and the time step is fixed to $\delta t = 10^{-4}$, up to the final time $T = 4$. The flow entesr through the left boundary, so we use a Dirichlet boundary condition: $\rho = 1.4$, $\mathbf{u} = (3, 0)$ and $p = 1$. For the top and bottom walls, we use zero flux boundary conditions. A free boundary condition is used for the right section.

We compare in Fig. 9 the results obtained with the first order scheme and the MUSCL scheme. The discontinuity line appears more clearly with the MUSCL scheme and the solution is closer to the one in [53]. A completer: plus de points ou methode d ordre plus elevee chez eux?

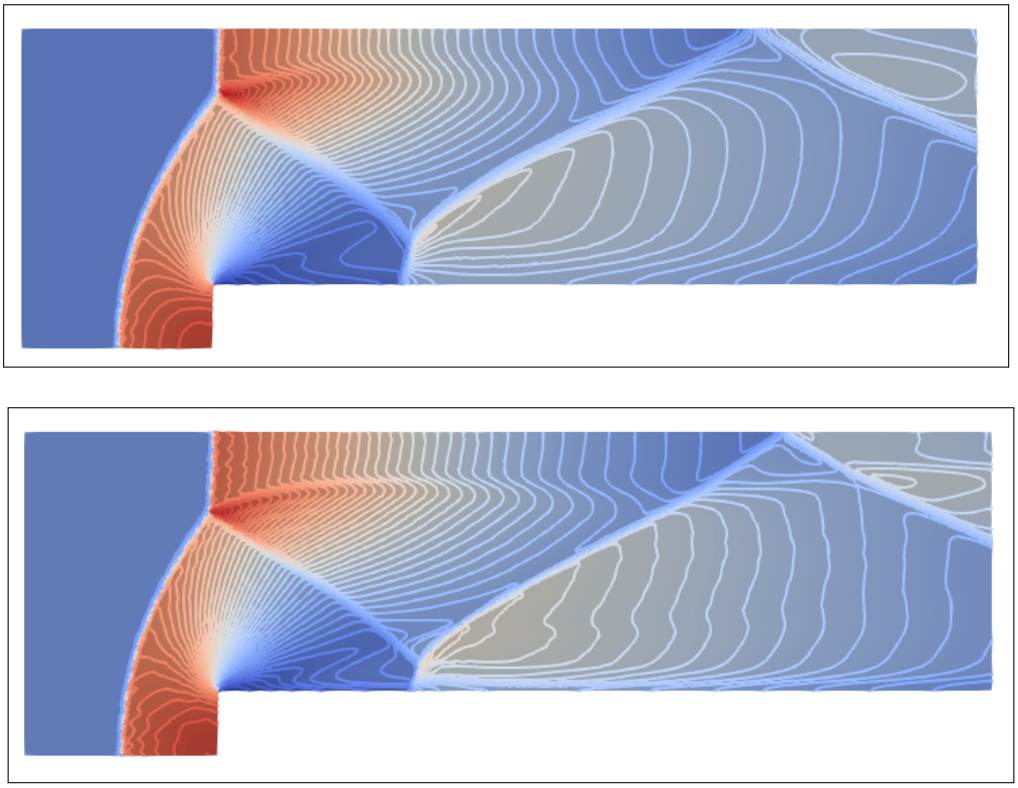

Figure 9: Density with 50 contour lines for the first order scheme (top) and MUSCL scheme (bottom)

5.2.3 2d Noh problem

We turn to the 2textscd Noh problem described in [45]. The main domain is a disk of radius 0.4 filled with a gas ($\gamma = 5/3$) initiated with $\rho_0 = 1$, $e_0 = 0$, and $\mathbf{u}_0(x, y) = \left(-x/\sqrt{x^2+y^2}, -y/\sqrt{x^2+y^2}\right)$.

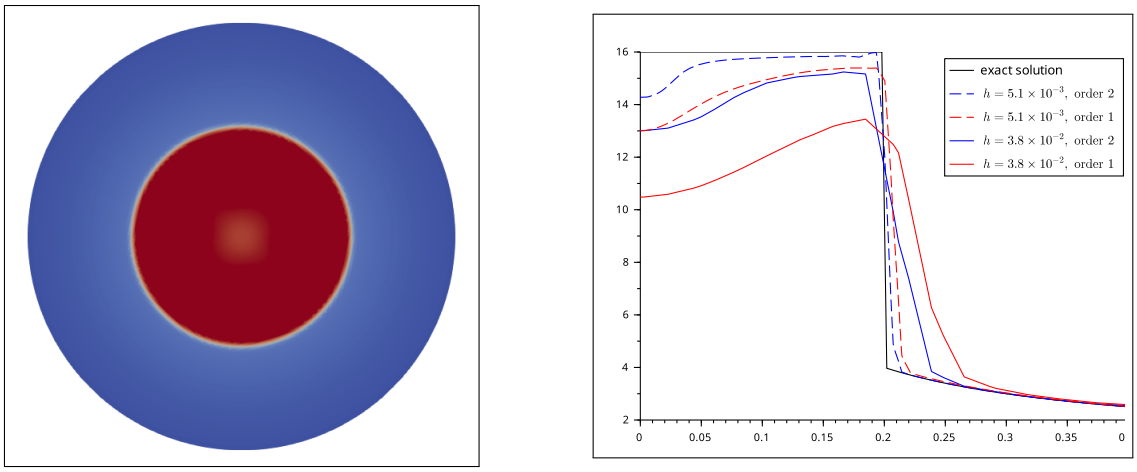

Figure 10: Density at time 0.6 (on the left) and horizontal cutline from the origin (on the right)

A shock wave is generated at the origin and expands (Fig. 10-left shows the obtained solution at time $t = 0.6$). The exact solution at time $t = 0.6$ is

$$(\rho, e, u) = \begin{cases} \left(\rho = 16, e = \frac{1}{2}, \mathbf{u} = \mathbf{0}\right) & \text{if } r < 0.2, \\ \left(\rho = 1 + \frac{3}{5r}, e = 0, \mathbf{u} = u_0\right) & \text{if } r > 0.2, \end{cases}$$

where $r = \sqrt{x^2 + y^2}$.

Fig.10-left shows the density of the solution obtained with the MUSCL scheme at $t = 0.6$. On Fig.10-right, we compare horizontal cutlines starting from the center of the disk till the boundary of solutions obtained with the first order scheme and the MUSCL scheme for two different mesh size h ($h = 3.8 \times 10^{-2}$ and $h = 5.1 \times 10^{-3}$). Commenter, comparer, parler du decrochage a gauche... The simulations in [45] are done on the quarter of the disk with symmetry conditions on the horizontal and vertical boundary, which reduces the computational effort. Moreover, the mesh is refined near the origin to obtain a better resolution for the shock.

For the MUSCL scheme, doing the simulation on the quarter disk might cause symmetry issues near the boundary, as explaioned in [50]; otherwise it is still possible to must impose the exact solution on the boundaries. Instead, here we have performed simulations on the full disk and without mesh-refinement near the origin. We clearly see in Fig. 10 the amelioration of the numerical solution for the MUSCL scheme for different meshes.

5.2.4 Triple point problem

The following simulation is inspired from [45, 55]. We consider a 2D Riemann problem with three states, and two materials. The situation generates vorticity. The computational domain is the square $[0, 7] \times [0, 3]$. Initially, the velocity is zero $\mathbf{u} = 0$ and the domain splits into three separate regions. Each region has an ideal gas equation of state. Initial conditions and material properties are specified according to the following diagram:

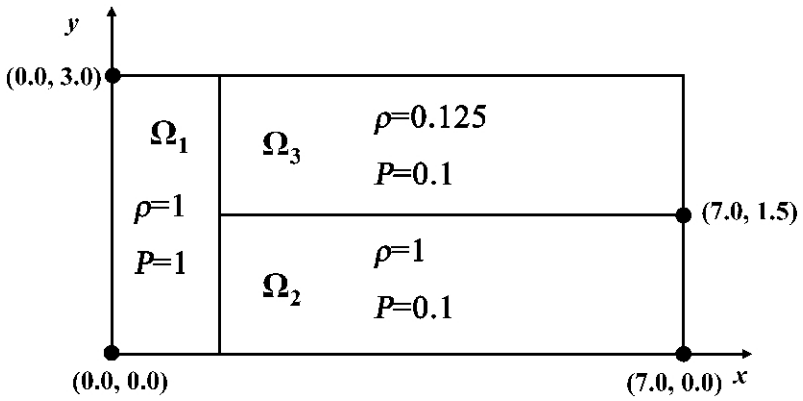

Figure 11: The triple point problem initial conditions

Fig. 12 displays the numerical density at time $T = 5$ for the first order scheme (top) and the MUSCL scheme (bottom). We clearly see the amelioration provided by the MUSCL scheme, especially in the vorticity zone.

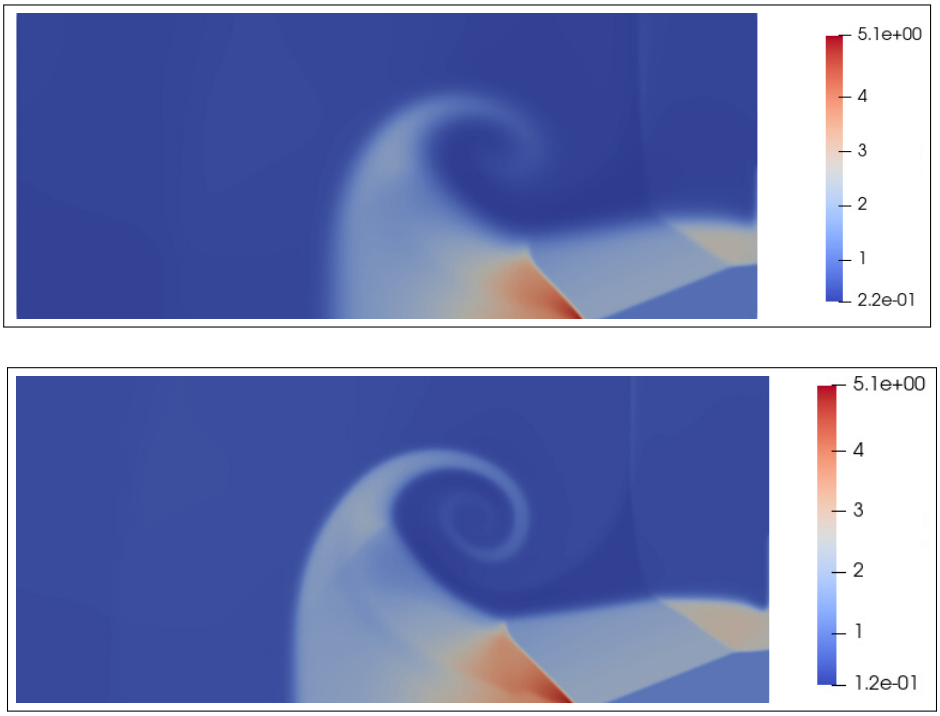

Figure 12: Density with 50 contour lines for the first order scheme (top) and MUSCL scheme (bottom)

.

6 Conclusion

References

[1] Nina Aguillon. *Problèmes d'interfaces et couplages singuliers dans les systèmes hyperboliques: analyse et analyse numérique*. PhD thesis, Paris 11, 2014.

[2] Timothy Barth and Dennis Jespersen. The design and application of upwind schemes on unstructured meshes. In *27th Aerospace sciences meeting*, page 366, 1989.

[3] Paul Batten, Claire Lambert, and Derek M. Causon. Positively conservative high-resolution convection schemes for unstructured elements. *International Journal for Numerical Methods in Engineering*, 39(11):1821–1838, 1996.

[4] Marsha Berger, Michael J. Aftosmis, and Scott M. Murman. Analysis of slope limiters on irregular grids. In *43rd AIAA Aerospace Sciences Meeting*, 2005. NAS Technical Report NAS-05-007.

[5] Florent Berthelin, Thierry Goudon, and Sebastian Minjeaud. Kinetic schemes on staggered grids for barotropic Euler models: entropy-stability analysis. *Mathematics of Computation*, 84(295):2221–2262, 2015.

[6] Florent Berthelin, Thierry Goudon, and Sebastian Minjeaud. Multifluid flows: a kinetic approach. *Journal of Scientific Computing*, 66:792–824, 2016.

[7] Christophe Berthon, Yves Coudière, and Vivien Desveaux. Second-order MUSCL schemes based on dual mesh gradient reconstruction (DMGR). *ESAIM: Mathematical Modelling and Numerical Analysis*, 48(2):583–602, 2014.

[8] F. Bouchut. *Nonlinear stability of finite volume methods for hyperbolic conservation laws and well-balanced schemes for sources*. Frontiers in Mathematics. Birkhäuser, 2004.

[9] Franck Boyer, Stella Krell, and Flore Nabet. Inf-Sup stability of the discrete duality finite volume method for the 2D Stokes problem. *Mathematics of Computation*, 84(296):2705–2742, 2015.

[10] Thierry Buffard and Stéphane Clain. Monoslope and multislope MUSCL methods for unstructured meshes. *Journal of Computational Physics*, 229(10):3745–3776, 2010.

[11] Caterina Calgaro, Emile Chane-Kane, Emmanuel Creusé, and Thierry Goudon. L^∞-stability of vertex-based MUSCL finite volume schemes on unstructured grids: Simulation of incompressible flows with high density ratios. *Journal of Computational Physics*, 229(17):6027–6046, 2010.

[12] Caterina Calgaro, Emmanuel Creusé, and Thierry Goudon. An hybrid finite volume–finite element method for variable density incompressible flows. *Journal of Computational Physics*, 227(9):4671–4696, 2008.

[13] Stéphane Clain and Vivien Clauzon. L^∞ stability of the MUSCL methods. *Numerische Mathematik*, 116:31–64, 2010.

[14] Vivien Clauzon. *Analyse de schémas d'ordre élevé pour les écoulements compressibles. Application à la simulation numérique d'une torche à plasma.* PhD thesis, Université Blaise Pascal-Clermont-Ferrand II, 2008.

[15] Phillip Colella. Multidimensional upwind methods for hyperbolic conservation laws. *Journal of Computational Physics*, 87(1):171–200, 1990.

[16] Sarah Delcourte and Pascal Omnes. A discrete duality finite volume discretization of the vorticity-velocity-pressure Stokes problem on almost arbitrary two-dimensional grids. *Numerical Methods for Partial Differential Equations*, 31(1):1–30, 2015.

[17] Stéphane Dellacherie. Analysis of Godunov type schemes applied to the compressible Euler system at low Mach number. *Journal of Computational Physics*, 229(4):978–1016, 2010.

[18] Stéphane Dellacherie, Pascal Omnes, and Felix Rieper. The influence of cell geometry on the Godunov scheme applied to the linear wave equation. *Journal of Computational Physics*, 229(14):5315–5338, 2010.

[19] Alain Dervieux and Jean-Antoine Desideri. Compressible flow solvers using unstructured grids. *NASA STI/Recon Technical Report N*, 94:17531, 1992.

[20] Komla Domelevo and Pascal Omnes. A finite volume method for the Laplace equation on almost arbitrary two-dimensional grids. *ESAIM: Mathematical Modelling and Numerical Analysis*, 39(6):1203–1249, 2005.

[21] Arnaud Duran, Jean-Paul Vila, and Rémy Baraille. Energy-stable staggered schemes for the Shallow Water equations. *Journal of Computational Physics*, 401:109051, 2020.

[22] R. Eymard, T. Gallouët, and R. Herbin. Finite volume methods. In Ph Ciarlet and J.L. Lions, editors, *Handbook of numerical analysis, Vol. VII*, Handb. Numer. Anal., VII, pages 715–1022. North-Holland, Amsterdam, 2000.

[23] Laura Gastaldo, Raphaèle Herbin, Jean-Claude Latché, and Nicolas Therme. A MUSCL-type segregated–explicit staggered scheme for the Euler equations. *Computers & Fluids*, 175:91–110, 2018.

[24] E. Godlewski and P.-A. Raviart. *Numerical approximation of hyperbolic systems of conservation laws*, volume 118 of *Applied Mathematical Sciences*. Springer, New-York, 1996.

[25] J. B. Goodman and R. J. LeVeque. On the accuracy of stable schemes for 2D conservation laws. *Math. Comp.*, 45(171):15–21, 1985.

[26] Thierry Goudon and Stella Krell. A DDFV scheme for incompressible Navier-Stokes equations with variable density. In *Finite Volumes for Complex Applications VII-Elliptic, Parabolic and Hyperbolic Problems: FVCA 7, Berlin, June 2014*, pages 627–635. Springer, 2014.

[27] Thierry Goudon, Stella Krell, and Giulia Lissoni. DDFV method for Navier–Stokes problem with outflow boundary conditions. *Numerische Mathematik*, 142:55–102, 2019.

[28] Thierry Goudon, Julie Llobell, and Sebastian Minjeaud. An explicit MUSCL scheme on staggered grids with kinetic-like fluxes for the barotropic and full Euler system. *Communications in Computational Physics*, 27(3):672–724, 2020.

[29] Thierry Goudon, Julie Llobell, and Sebastian Minjeaud. An explicit finite volume scheme on staggered grids for the Euler equations: Unstructured meshes, stability analysis, and energy conservation. *International Journal for Numerical Methods in Fluids*, 94(1):76–119, 2022.

[30] Hervé Guillard and Angelo Murrone. On the behavior of upwind schemes in the low Mach number limit: II. Godunov type schemes. *Computers & fluids*, 33(4):655–675, 2004.

[31] Hervé Guillard and Cécile Viozat. On the behaviour of upwind schemes in the low Mach number limit. *Computers & fluids*, 28(1):63–86, 1999.

[32] Putu Harry Gunawan and Sri Redjeki Pudjaprasetya. Explicit staggered grid scheme for rotating shallow water equations on geostrophic flows. *Progress in Computational Fluid Dynamics*, 8(1):46–55, 2018.

[33] Raphaèle Herbin, Walid Kheriji, and Jean-Claude Latché. Staggered schemes for all speed flows. In *ESAIM: Proceedings*, volume 35, pages 122–150, 2011.

[34] Raphaèle Herbin, J-C Latché, and Trung Tan Nguyen. Explicit staggered schemes for the compressible Euler equations. In *ESAIM: Proceedings*, volume 40, pages 83–102. EDP Sciences, 2013.

[35] Raphaèle. Herbin, Jean-Claude Latché, and Trung Tan Nguyen. Consistent segregated staggered schemes with explicit steps for the isentropic and full Euler equations. *ESAIM-Math. Model. Numer. Anal.*, 52(3):893–944, 2018.

[36] Francois Hermeline. A finite volume method for the approximation of diffusion operators on distorted meshes. *Journal of computational Physics*, 160(2):481–499, 2000.

[37] Matthew E. Hubbard. Multidimensional slope limiters for MUSCL-type finite volume schemes on unstructured grids. *Journal of Computational Physics*, 155(1):54–74, 1999.

[38] Anthony Jameson and D Mavriplis. Finite volume solution of the two-dimensional Euler equations on a regular triangular mesh. *AIAA journal*, 24(4):611–618, 1986.

[39] Stella Krell. Stabilized DDFV schemes for Stokes problem with variable viscosity on general 2D meshes. *Numerical Methods for Partial Differential Equations*, 27(6):1666–1706, 2011.

[40] Clément Le Touze, Angelo Murrone, and Herve Guillard. Multislope MUSCL method for general unstructured meshes. *Journal of Computational Physics*, 284:389–418, 2015.

[41] R. J. LeVeque. *Finite volume methods for hyperbolic problems*. Cambridge Texts in Applied Mathematics. Cambridge University Press, Cambridge, 2002.

[42] Wanai Li, Yu-Xin Ren, Guodong Lei, and Hong Luo. The multi-dimensional limiters for solving hyperbolic conservation laws on unstructured grids. *Journal of Computational Physics*, 230(21):7775–7795, 2011.

[43] Meng-Sing Liou. A sequel to AUSM: AUSM+. *Journal of computational Physics*, 129(2):364–382, 1996.

[44] Meng-Sing Liou and Christopher J Steffen Jr. A new flux splitting scheme. *Journal of Computational physics*, 107(1):23–39, 1993.

[45] Raphaël Loubere. Validation test case suite for compressible hydrodynamics computation. *Unpublished notes, Los Alamos National Laboratory*, 39, 2005.

[46] Benoît Perthame. *Kinetic formulation of conservation laws*, volume 21 of *Oxford Lecture Series in Math. and its Appl.* Oxford Univ. Press, 2002.

[47] Peter K Sweby. High resolution schemes using flux limiters for hyperbolic conservation laws. *SIAM journal on Numerical Analysis*, 21(5):995–1011, 1984.

[48] Nicolas Therme. *Schémas numériques pour la simulation de l'explosion*. PhD thesis, Aix-Marseille, 2015.

[49] E. F. Toro. *Riemann solvers and numerical methods for fluid dynamics*. Springer-Verlag, Berlin, third edition, 2009.

[50] Eleuterio Francisco Toro et al. Anomalies of conservative methods: analysis, numerical evidence and possible cures. *Computational Fluid Dynamics Journal*, 11(2):128–143, 2002.

[51] Bram Van Leer. Towards the ultimate conservative difference scheme. V. a second-order sequel to Godunov's method. *Journal of computational Physics*, 32(1):101–136, 1979.

[52] John von Neumann and Robert D. Richtmyer. A method for the numerical calculation of hydrodynamics shocks. *J. Appl. Phys.*, 21:232–237, 1950.

[53] Paul Woodward and Phillip Colella. The numerical simulation of two-dimensional fluid flow with strong shocks. *Journal of computational physics*, 54(1):115–173, 1984.

[54] Phillip Woodward and Phillip Colella. The numerical simulation of two-dimensional fluid flow with strong shocks. *J. Comput. Phys.*, 54(1):115–173, 1984.

[55] Chao Zhang and Igor Menshov. Eulerian model for simulating multi-fluid flows with an arbitrary number of immiscible compressible components. *Journal of Scientific Computing*, 83(2):31, 2020.